water

MDPI

Article

A Growing Heavy Runoff Fingerprint of Climate Changes in the Sacramento San Joaquin Watershed

Lu Su [1], Daniel R. Cayan [1,*], David W. Pierce [1], Benjamin Bass [2], Michael D. Dettinger [1], Alexander Gershunov [1] and Ming Pan [1]

[1] Scripps Institution of Oceanography, University of California San Diego, 8622 Kennel Way, La Jolla, CA 92037, USA; l3su@ucsd.edu (L.S.); dpierce@ucsd.edu (D.W.P.); mddettinger@gmail.com (M.D.D.); agershunov@ucsd.edu (A.G.); m3pan@ucsd.edu (M.P.)
[2] Department of Atmospheric and Oceanic Sciences, University of California Los Angeles, Maths Science Building, 520 Portola Plaza, Los Angeles, CA 90095, USA; benjamin.bass@bsc.es
* Correspondence: dcayan@ucsd.edu

Abstract

As climate warms in California mountain zones, shifts in runoff will occur, not only in its seasonal mean structure but also in the form of its daily runoff events. This transition will modify a historical hydroclimate where large precipitation events already have exceptionally strong influence. Although the intensification of heavy precipitation events has been studied extensively, climate change-driven shifts in heavy runoff events have received less attention. This investigation considers future changes in high-percentile daily runoff over complex topography, in response to future climate warming and occasionally heavier precipitation events. The study is based upon VIC hydrological simulations driven by 13 LOCA2-downscaled CMIP6 climate projections. The study domain covers 210 diverse lower- to higher-elevation catchments that drain into the Sacramento/San Joaquin Delta Watershed, in northern and central California, which provides many ecosystem services and supplies a major portion of the state's water. Under a relatively high-emissions climate change scenario increase in daily runoff events that reach or exceed the 98th historical percentile are found, contributing nearly twice their cumulative volume relative to the 1952–2014 historical period. This increase occurs unevenly across the Delta Watershed, dominated by daily runoff events in medium-elevation mixed rain/snow catchments whose future occurrence increases by 179% of their historical mean. Highest-elevation catchments transition toward a winter/earlier spring runoff regime where 98th percentile occurrences decline to 62% of historical occurrences as warming causes snowpack to recede and historically familiar spring–summer snowmelt peaks fade. High-percentile runoff events are more likely during wet years and notably lacking during dry years. The results indicate a future with greater flood risk. Runoff days reaching or exceeding the historical 99.9th percentile (~2.7 year return period) occur more often across all elevations, likely in response to warm winter storms. These increases are especially impactful in medium and high elevations, where 99.9 percentile runoff days occur more than 240% more often than in the historical period and contribute more than 280% to annual runoff.

Keywords: climate change; runoff; extreme precipitation; snowpack; flooding; flood risk; water resources; California

Check for updates

Academic Editors: Christos S. Akratos and Athanasios Loukas

Received: 1 July 2026
Revised: 10 October 2026
Accepted: 13 October 2026
Published: 29 October 2026

Copyright: © 2026 by the authors. Licensee MDPI, Basel, Switzerland. This article is an open access article distributed under the terms and conditions of the Creative Commons Attribution (CC BY) license.

1. Introduction

One prominent change expected under projected climate change in continental regions is that, with additional global warming, heavy precipitation will become more intense [1–4]. In California, modeled future precipitation is projected to undergo a regime shift [3]. This transition results in fewer numbers of wet days within a year, a somewhat narrower wet season, and occasionally greater, extremely wet storm days [1–3,5,6]. Related to these changes are wider swings between very wet and very dry years [2,7,8], heightening both flood risk and drought severity across the state, as described in the California Fourth Climate Change Assessment [9].

Historically, the occurrence or absence of a few heavy storm events per year has an unusually large influence on the volume of annual and multiannual precipitation in California [10,11]. Even though climate models project inconsistent or model-dependent changes in overall precipitation totals, the disproportionate impact of heavy precipitation events is projected to grow [11], with climate models showing precipitation regime change [3] through storm track migration and thermodynamic changes. The projected future hydroclimate shifts toward fewer wet days overall but with occasional enriched storm totals as the atmosphere gains more humidity. The increase in the upper tail of the distribution of daily precipitation [1,12,13] in the future in California can be attributed to enhanced atmospheric river events [3,6,14,15]. Associated climate change-related increases in bulk characteristics of runoff extremes have also been described [16–19].

The focus of this study concerns possible shifts in high-percentile daily runoff events within the Sacramento/San Joaquin watershed (hereafter the Delta Watershed; Figure 1). The Delta Watershed is chosen because of its diverse physical characteristics, vital water supply functions, and the vulnerabilities it presents to natural and human systems. As employed in this study, the Delta Watershed amounts to approximately 18% of California's land area but averages nearly one-third of the entire statewide precipitation and generates a disproportionate amount of California's runoff. This watershed supplies a major share of the water used by California's agriculture, residential and commercial users, and provides water to ecosystems in the upstream catchments, the Delta and the downstream San Francisco Bay [20,21]. The Sacramento/San Joaquin watershed collects runoff from throughout the watershed but is vulnerable to climate change [22,23]. The Delta Watershed is well situated to generate high runoff events, with south to north mountain terrain oriented normal to moist westerly or southwesterly storm winds that often create high orographic amplification of storm precipitation [6,24]. Within the relatively warm Pacific air masses that determine the climate of this watershed, winter and spring snow losses and earlier snowmelt are already observed at a surprising pace [25–32]. Shifts in snow-driven hydrology are projected to continue rapidly as the climate warms [33–39]. Furthermore, although annual runoff rose only modestly in hydrologically modeled Coupled Model Intercomparison Project Phase 3 (CMIP3) projections, Das et al. [17] reported a 50–100% increase in multi-day rain-on-snow flood volumes by late century. Similarly, in a later set of hydrologically modeled CMIP5 projections, Knowles et al. found that 100-year daily flood magnitudes in the Delta Watershed could more than double by late century [18]. These findings kindle further questions about how heavy runoff changes might occur over the complex topography within this regional watershed.

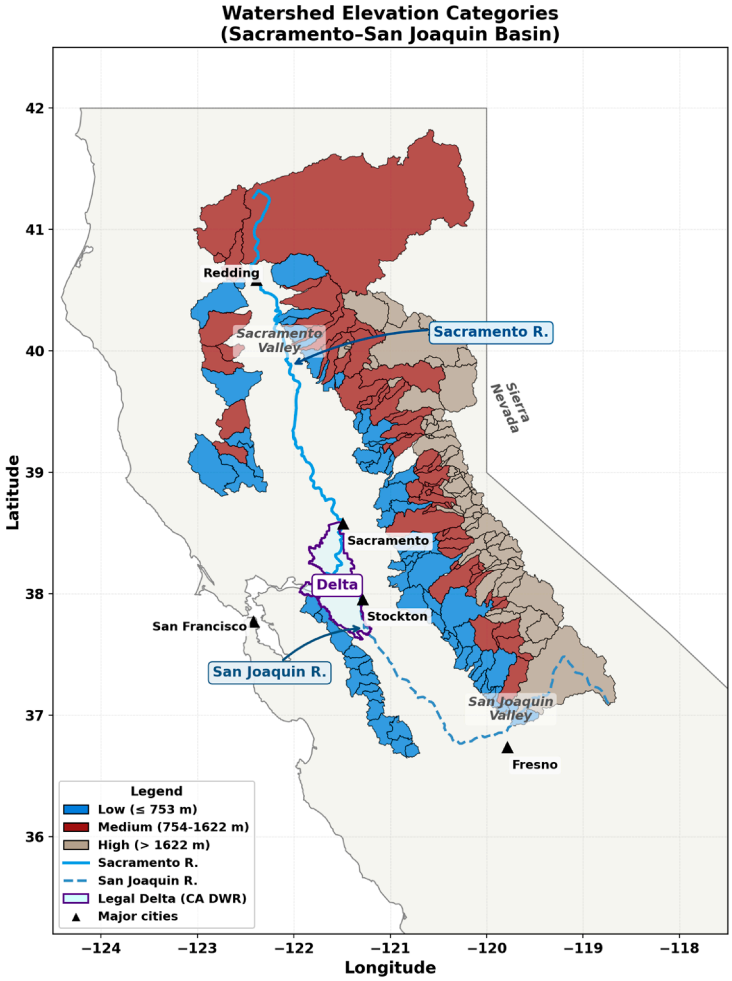


Figure 1. The 210 upstream catchments that feed freshwater into the Delta. Shading delineates three elevation bands—low (blue), medium (red), and high (taupe), as defined by mean elevation of catchments.

Clearly, high-intensity daily runoff events will be an increasingly important feature of the region's projected future hydroclimate, but changes in runoff pulses have not received the scrutiny that has been given to intensifying heavy daily precipitation events. Here, considering the many individual catchments that contribute to the Delta Watershed, we undertake a deeper dive into the 21st Century evolution of increased high precipitation events and their presumed association with high daily runoff. Our investigation is based upon a set of hydrologically modeled climate scenarios run under a set of downscaled CMIP6 climate model projections, which were downscaled with special attention to represent extreme events. While increases in heavy precipitation would very likely produce increased daily runoff events, the Delta Watershed consists of diverse physiographic characteristics and climate that will likely dampen this hydrological response in some cases and amplify it in others. This study will consider the following questions:

- How will runoff responses vary across elevations?
- How might extreme-runoff changes occur over the water year calendar?
- How might contributions to annual total runoff from extreme daily events change?
- Given the region's high interannual variability of precipitation, how might event-scale runoff changes differ in wet years from those in dry years?

To address these questions, the paper presents Data and Methods in Section 2, Results in Section 3, a Discussion in Section 4, and Conclusions in Section 5.

2. Data and Methods

2.1. Study Region

The Delta Watershed study region, shown as the colored portion of Figure 1, is represented by 210 catchments, totaling roughly 75,000 km^2, that feed into the Sacramento/San Joaquin Delta Watershed. These 210 catchments, which constitute the entire set of rim catchments that feed into the Delta, are chosen because of their dominant contribution to the region's water flows and because they cover much of the topographic and climatological range in the watershed. The part of the watershed on the floor of the Sacramento and San Joaquin Valley does receive precipitation and generates runoff, but it is smaller than that from the catchments upstream, and so this area is not included here. The Delta Watershed study region, roughly 75,000 km^2, draws nearly all of its waters from the westward slope of the Sierra Nevada range to the east and the eastward and southward slopes of the Coastal Range to the west and south. The 210 catchments lie between 36° N and 42° N, having mean elevations from near sea level to more than 2800 m.

2.2. VIC Hydrological Model

We employ the Variable Infiltration Capacity (VIC) model, a process-based macroscale, semi-distributed hydrological model that simulates land surface moisture and energy fluxes by solving the surface water and energy balance equations [40]. VIC was employed because of its applicability to hydroclimate change investigations. VIC has been widely applied to various major river basins [41,42] and is supported by a large international user community. In particular, relevant to the present study, a relatively highly resolved 3 km spatial resolution version of VIC historical and future period runs over California was assessed [19], being one of two hydrological models that were employed for California energy interests and the recent California Fifth Climate Change Assessment [43].

Results here are obtained from the VIC version 4.1.2 run in energy balance mode that was configured for California climate change evaluation at a spatial resolution of 1/32° in both latitude and longitude [19,44]. A calibration of VIC parameters was performed specifically for the California Climate Assessment project, and that version of VIC was employed in the present study. Prior to calibrating the VIC model parameters, an evaluation was conducted of the model's ability to simulate snow water equivalent (SWE) at 20 select SNOTEL sites across the western United States. This preliminary assessment was a crucial benchmarking step to ensure robust snowpack dynamics before fine-tuning hydrology, and our simulations demonstrated strong SWE performance [45]. With the snow simulation skills verified, the VIC model was run in energy balance mode using initial parameters based on Livneh et al.'s previous validation of model discharges over major CONUS river basins [40]. VIC parameters for California were calibrated using a global optimal calibration method called the Dynamically Dimensioned Search algorithm [46], following the methodology described in [19,45]. The soil and land cover parameters employed for VIC are those used by Su et al. [45]. The calibration was forced by a form of the historically reanalyzed meteorological dataset, ERA5-WRF-BC [47]. Simulated VIC runoff averaged over several west slope Sierra catchments was compared and adjusted to replicate multi-decade USGS stream gage records that were chosen based upon having minimal diversions and other manipulations in their upstream catchments. The calibration optimized the agreement between the VIC runoff and the observed streamflow at a daily time resolution via the Kling–Gupta Efficiency (KGE) metric [48] as an objective function [44,45]. The calibrated parameters then were extended to ungauged basins throughout California, including many of the numerous catchments in the Delta Watershed (Figure 1).

As a post-calibration check for this study, the combined annual (water year) runoff across 1952–2015 was assessed from the 210 VIC-generated rim basin catchments that

contribute to the Delta Watershed (Table 1). This annual runoff was correlated with the water year discharge from combined Sacramento River and San Joaquin River naturalized inflows produced by the California Department of Water Resources [49], resulting in a high (r = 0.97) correlation. Furthermore, evaluation of monthly historical runoff at 9 individual westward slope catchments within the Delta Watershed (Figure S1) over the 1952–2000 period that preceded the 2001–2020 calibration period yielded good skill and little reduction of performance from the calibration period across these catchments (Table S1a,d).

Table 1. VIC normalized Delta Watershed annual precipitation and annual runoff compared against the sum of California Department of Water Resources Sacramento and San Joaquin naturalized annual discharge and NOAA climate division annual precipitation, showing correlation (r), root mean square error (RMSE) and Kling–Gupta Efficiency (KGE). The 2001–2020 span is the period over which the VIC model was calibrated, and 1952–2000 is independent of that calibration period, except for a few watersheds having limited records during 2001–2020.

Period	Variable	r	RMSE	KGE
2001–2020	Precipitation	0.989	0.054	0.864
2001–2020	Runoff	0.993	0.051	0.845
1952–2000	Precipitation	0.967	0.080	0.851
1952–2000	Runoff	0.974	0.079	0.836

To drive VIC in subsequent simulations, daily LOCA2 downscaled global climate model meteorological forcings were disaggregated to a 3 h timestep using the MTCLIM algorithm [19,50]. The resulting 3 h forcing dataset includes precipitation, temperature, atmospheric pressure, specific humidity, incoming shortwave and longwave radiation, and the zonal and meridional wind components. For each of the 13 projections (Table S2), longwave radiation was estimated using the MTCLIM formulation [51]. For six of the global climate models (GCMs) that lack some required variables, MTCLIM-estimated variables or historical climatological wind data were used (see Table S2 for details). In the analyses conducted here, VIC outputs of daily runoff, snow water equivalent (SWE) and soil moisture are the primary outputs of interest.

2.3. CMIP6 Climate Change Projections

The dataset employed in the present study consists of 13 hydrological projections modeled by VIC over the period of 1952–2099 water years. The projections are driven by 13 Localized Constructed Analogs version 2 (LOCA2) downscaled Coupled Model Intercomparison Project, Phase 6 (CMIP6) models (Table S2). These models were selected [52] on the basis of good performance in their historical representation of atmospheric circulation structures relevant to California climate and weather variations and of regional temperature and precipitation statistics within California. The climate projections are all run under the SSP370 scenario. SSP370 was employed because it is a plausible scenario that includes regional rivalry and relatively high fossil-fuel dependency. Although multiple ensemble members were provided by many of the GCMs, only one ensemble member for each GCM was employed to avoid overreliance on GCMs with higher numbers of ensemble members dominating the results. Previous evaluations [53,54] have demonstrated that variation across models is one of the major sources of projection uncertainty in the several-decade future, more so than internal variability across model ensemble member variants, so the 13-member model set is likely to bracket much of the variation space.

2.4. LOCA2 Downscaled Meteorology

The meteorological driver for the hydrological model is the LOCA2-Hybrid dataset for California (https://loca.ucsd.edu/loca-version-2-for-california-ca-may-2023/, accessed 1 May 2023), which was developed for the California energy utility community and to support the Fifth California Climate Assessment (https://www.lci.ca.gov/wp-content/uploads/20260108-ClimateChangeAssessment-Factsheet.pdf (accessed on 30 June 2026)). The LOCA2-Hybrid data were used because LOCA2 downscaling performs reasonably well in replicating historical climate, including extreme daily temperature and precipitation [12,36], and it provides projected meteorology for a large set of CMIP6 models run according to the SSP370 scenario. The LOCA2-Hybrid methodology is a statistical-dynamical approach using dynamically downscaled WRF data as the training dataset [47].

This study does not directly employ historically observed meteorological data to run VIC. Instead, the set of LOCA2-generated historical (1950–2014) meteorological data for the respective GCMs is employed, which is compatible with the hydrological modeled results from the same model's projected future period (2015–2100). At the same time, the historical projections have climatological means and variability that are consistent with observational statistics through the LOCA2-hybrid bias correction [47,55], wherein CMIP6 GCM-projected changes, by quantile and by season, were preserved. The gridded, observationally based dataset used in the bias correction was a set of results from the ERA5-WRF-BC downscaled reanalysis dataset, a 3 km WRF dynamically downscaled version of the ERA5 global reanalysis that was subsequently bias-corrected to observations from meteorological stations that had at least 30 years of data available [56].

The LOCA2-hybrid downscaling is especially designed to capture extremes in daily precipitation and temperatures. The LOCA2-hybrid technique avoids the stationarity assumption that historical weather patterns will continue to be valid in the future, which underlies many statistical downscaling schemes. LOCA2 couples the statistical analogue matching approach of LOCA [57] with a daily weather pattern library obtained from a dynamically downscaled model containing information about the historical and future climate [58]. The period covered by the GCM-WRF runs extends to the year 2099, providing an estimate of future climate and weather patterns covering the 21st Century.

2.5. Hydrological Model Projections

The set of 13 CMIP6 projections is used to investigate changes in the hydroclimate variables across the 1952–2099 time span, comparing results from its future period against its historical period. As noted, the LOCA2 downscaled meteorological forcing data were bias-corrected, but no further bias correction was applied to the VIC hydrological model output. A schematic of the experiments is shown in Figure 2.

The GCM climate projections are SSP370 scenario simulations (Table S2). Thirteen GCMs were chosen based on statistical evaluations that identified them as the best performers for simulating important aspects of California's climate, including salient large-scale dynamics and regional climate statistics [52]. Additionally, these GCM runs met a criterion that their outputs include the meteorological variables (including daily near-surface specific humidity) required for hydrological modeling. A spin-up period from January 1950 through October 1951 was implemented to allow the VIC model to reach hydrological equilibrium, so the data series begins 1 October 1951 (VIC data accessed 15 July 2023). Hence, the VIC daily data series includes water years 1952–2014 as its historical period, and water years 2015–2099 as the projected future period.

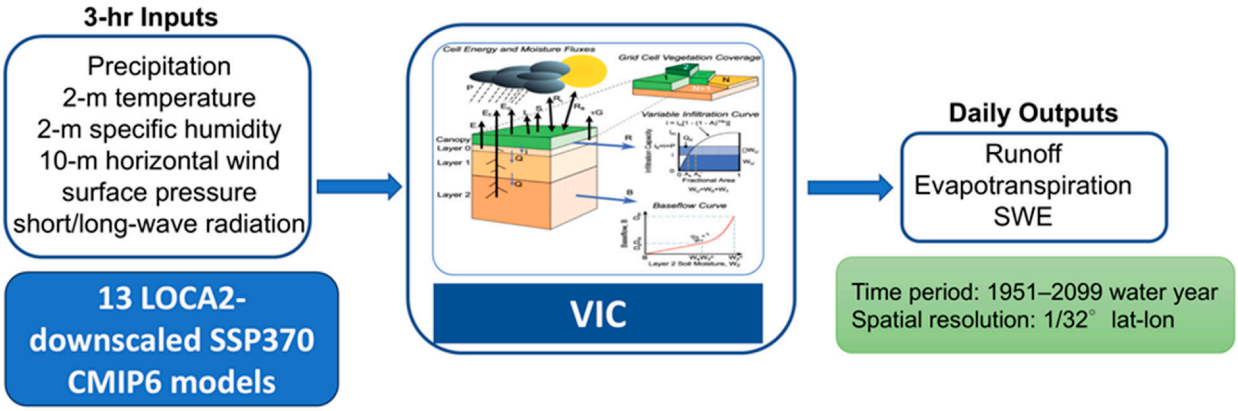


Figure 2. Schematic diagram of the LOCA downscaled CMIP6-to-VIC hydrological model experiments.

2.6. Climatological Periods

In keeping with California's wet boreal winter and dry summer climate, annual data are shown by water year, 1 October to 30 September. Several analyses employ aggregated measures within the 2037–2099 future period to compare with those from the equal 63-year (1952–2014) historical period. To investigate a more resolved time evolution, some additional analyses of the entire (1952–2099) time series are conducted to illustrate changes continuously across the 21st Century, and a few analyses employ 30-year aggregated data over early historical (1952–1981), recent historical (1991–2020), mid-21st Century (2031–2060) and late-21st Century (2071–2100) epochs.

2.7. Low-, Medium- and High-Elevation Catchments

For analysis, catchments are stratified by basin-mean elevation into three equally occurring bands (equal numbers of catchments, not equal area): low (≤753 m), medium (753–1622 m) and high (>1622 m), shown in Figure 1 and described in Table 2. To compare changes across elevations, these bands were structured to include equal numbers of catchments; as shown in Table 1. These zones do not contain equal areas. Medium elevation catchments encompass nearly half of the area of the entire Delta Watershed. Notably, precipitation and runoff grade upwards with elevation (Table 2 and Table S2), and estimated runoff efficiency (ratio of annual runoff/precipitation) ranges from an average of 0.32 in low-elevation catchments to nearly double that, 0.59, in high-elevation catchments. The pronounced seasonality and magnitudes of historical and future mean runoff from these elevation zones are shown in Figure 3. Mean annual totals of the three elevation bands and the whole Delta Watershed are listed in Table 2.

Table 2. Delta Watershed temperature, precipitation and runoff characteristics.

Elevation Class	Mean Elevation (m)	Area (km^2)	Mean Annual Temperature (°C)	Mean Annual Precipitation (10^9 m^3)	Avg Annual Runoff (10^9 m^3)
Low	524	19,391	18.3	14.3	4.6
Medium	1275	36,800	13.6	40.5	19.9
High	2030	18,821	9.4	21.3	12.6
Whole	1270	75,012	13.7	76.1	37.1

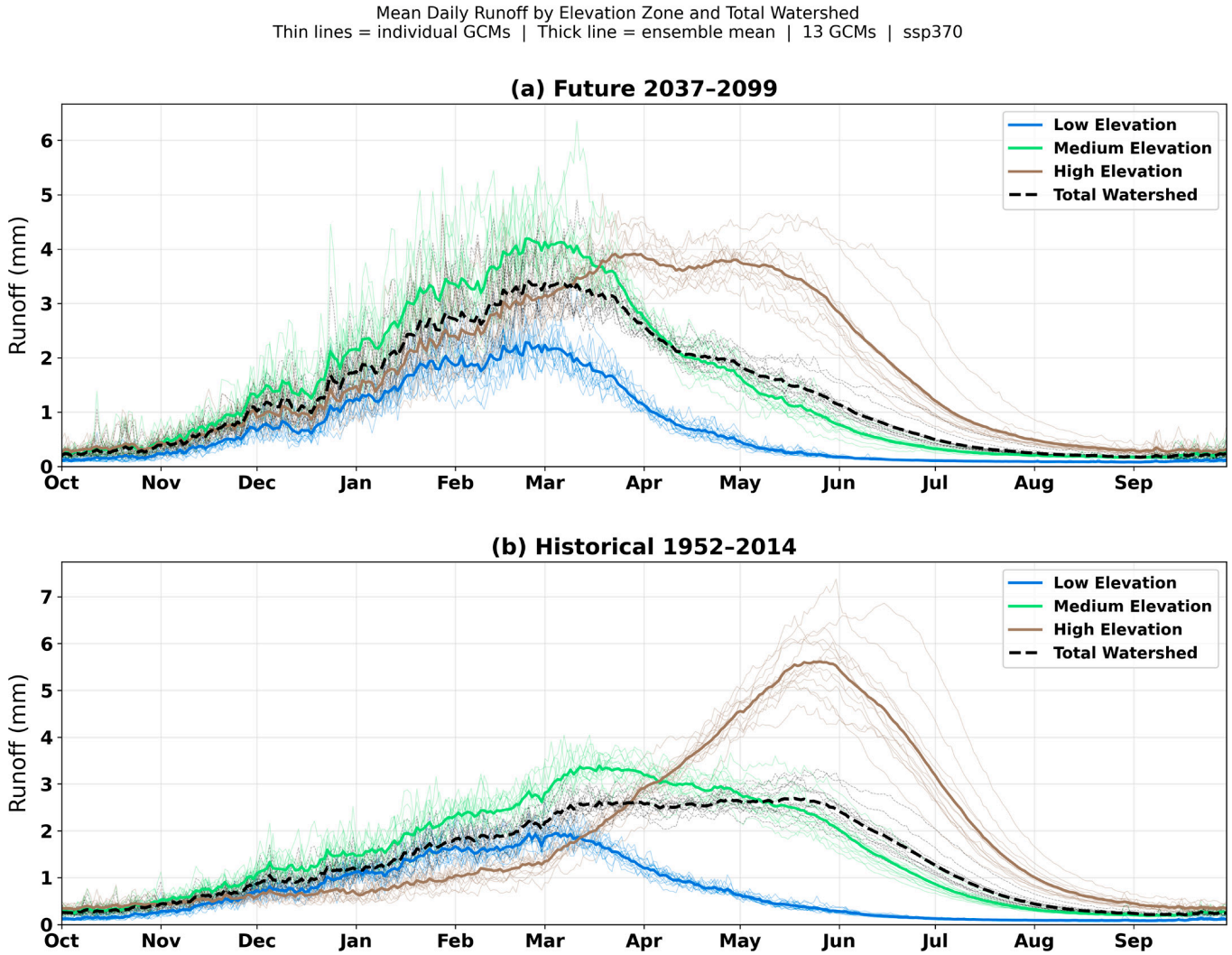


Figure 3. Mean runoff for Delta Watershed (dashed), low- (blue), medium- (green) and high-elevation catchments (brown) for 1952–2014 historical (**b**) and 2037–2099 future (**a**) periods.

2.8. Hydroclimate Measures, Percentile Thresholds and Year Types

Hydroclimate measures are determined for each VIC 3 km grid cell and aggregated over selected areas, namely the whole watershed, the sets of low-elevation, medium-elevation, and high-elevation catchments, for each of the 210 catchments of the Delta Watershed.

The runoff variable in this study is VIC total runoff, the sum of outflow through surface and subsurface pathways, at daily time increments. Other hydroclimate measures considered here are water year temperature (Tann), water year precipitation (Pann), water year runoff (Qann), April 1 snow water equivalent (SWEapr1), and the fraction of each water year's runoff attributed to rainfall and snowmelt, called Qrainfr and Qsnowfr, respectively. Each year's total runoff was multiplied by the fraction of the year's precipitation that falls as snow, and the fraction that falls as rain, to estimate the annual snow and rain fractions of runoff, respectively. Additionally, SWE change (in millimeters) is determined in association with high-percentile daily runoff events. The SWE change during an event is calculated as the difference day after minus day before a Q98 on Q99.9 runoff events. Antecedent 7-day SWE change is the difference of SWE the day before minus SWE 8 days before a runoff event.

In focusing on relatively heavy daily precipitation events, the primary precipitation measure considered here is daily precipitation equal to or exceeding the 95th percentile (P95). Also included is daily precipitation equal to or exceeding the 99.9th percentile (P99.9), along with daily precipitation P30y equaling or exceeding the 30-year recurrence interval. P95 and P99.9 thresholds are calculated using each model's historical period considering only wet days (≥1 mm of daily precipitation). Daily mean temperatures on P95 and P99.9 days are also considered. Roughly corresponding with the heavy daily precipitation events, the primary runoff measure is daily runoff equal to or exceeding the 98th percentile (Q98). The 98th percentile historical runoff threshold, which, on average, admits about 7 such days per year, was selected to be more closely matched in frequency than Q95 (on average, 18 days per year) with the occurrence of P95 daily "non-zero"+ precipitation events, which averages about 5 days per year. Also included, to more clearly evaluate unusually high runoff events, is daily runoff equal to or exceeding the 99.9th percentile (Q99.9), along with Q30y daily events equaling or exceeding the 10-year and 30-year recurrence intervals. Accumulated annual amounts of precipitation from all P95, P99.9, and P30y days and all Q98, Q99.9, and Q30y days are called P95sum/year, P99.9sum/year, P30ysum/year and Q98sum/year, Q99.9sum/year, and Q30ysum/year, respectively. Accumulated annual amounts of nonheavy precipitation from daily events less than the 95th percentile and runoff from daily events less than the 98th percentile are called P<95 and Q<98, respectively. Annual counts and the fraction of the annual total of various precipitation and runoff measures are labeled as "count/year" and "frac/annual". Q98 runoff intensity as a water-year average is calculated for each of the simulations as the annual volume contributed by Q98 days divided by their annual number and then averaged over the 13 simulations. Metric units (in millimeters or millimeters/year)] are used throughout. Historical and future values of these metrics are reported in Table A1 and Table S3.

In this study, dry, normal, and wet years are defined using the terciles of the 1952–2014 historical distributions. These are determined separately for each GCM projection wherein the lowest, middle and highest thirds of water-year precipitation are identified in each downscaled CMIP6 model simulation. Selected analyses also consider drier, near normal and wetter years defined by water-year precipitation that falls within the 10–30th, 40–60th, and 70–90th historical percentiles. Other definitions of wet and dry years are sometimes employed (e.g., quartiles or pentiles), but terciles are employed here to include more cases in dry and wet years and for comparable numbers in comparison with those in normal years.

3. Results

3.1. Future vs. Historical Hydroclimate Measures and Model Variability

Annual and daily high-percentile event means and variation of historical (1952–2014) and future (2037–2099) periods are shown in Appendix A, Table A1. Each of the mean measures is the average of that measure calculated separately for each of the 13 model simulations over the historical or the future time period. Also provided are two measures of variation, being the overall mean of each model's temporal variation over the respective time periods and the model-to-model variation of a given measure, calculated as the standard deviation of the 13 overall mean values of the given measure. Means and standard deviations are provided for the whole Delta Watershed and the low-, medium-, and high-elevation catchment subsets. Bold-faced future values identify cases where the 13-member future value result differs significantly from that of its 13-member historical counterpart, wherein significance is given when the t-value satisfies the $p < 0.05$ significance level.

As indicated in Table A1, nearly all of the high-percentile measures for the whole Delta Watershed and low-, medium- and high-elevation zones register statistically significant ($p < 0.05$) change in the future relative to the historical period. Temporal standard deviations of many of the measures are quite large relative to their mean values, reflecting the high interannual variability of precipitation and other hydroclimate measures [3,5,7] in the California region. In contrast, inter-model variation is often smaller than the future–historical difference, demonstrating a reasonably high degree of consistency across the 13 model simulations.

3.2. Precipitation Events and Changes

Whole Delta Watershed annual precipitation totals show a slight (2.5%) non-significant increase in the 2037–2099 future period (Table A1). But the volume of annual precipitation contributed by P95 days exhibits a 20.2% statistically significant increase. Over the historical period, cumulative daily precipitation from P95 days contributes 20% of the total annual volume of precipitation, rising in the future period to 23% of annual volume (Table A1). In the historical period, P95 days number, on average, 4.6 days/year, but, consistent with previous studies [10]; the P95 occurrences and volume contribution from the individual model projections vary considerably interannually, with average counts ranging from below 2 days to more than 7 days per year. P95 contributions to annual volume range from less than 10% to more than 30%. Impressively, in general agreement with results found by Dettinger [11], correlation of the P95 annual sum with annual precipitation r = 0.82) is nearly as strong as that of the considerably larger remainder of the annual total of non-heavy < P95 precipitation days (r = 0.89).

P95 volume contributions in the historical period are substantial, on average, accounting for 20% of total annual precipitation (Table A1). P95 historical volumes, on average, account for about 18% of total annual precipitation in low elevations, 20% in medium elevations and 22% in high-elevation catchments. Although observed precipitation extremes do not yet register increasing trends [3,6,59], P95 days, along with higher-percentile P99.9, P10y and P30y daily precipitation events, exhibit strong increases in the future period, consistent with previous studies [1,2,5]. Delta Watershed P95 counts increase by about 0.8days/year over their historical count. Moreover, the P95 volume fraction increases to 23% of the annual total precipitation, a shift toward greater contributions from heavier precipitation events even though annual mean precipitation increases less than 4% over its historical mean (Table A1).

The seasonal timing of heavy precipitation events is projected to experience only minor change in the future, illustrated in Figure 4 showing P95 events for medium-elevation catchments, consistent with Pierce et al. [12]. The future increase in heavy precipitation events occurs (Table A1) (consistently across the 13 models) to a degree that achieves a $p < 0.05$ significance level in each of the three elevation zones. Changes in P95 events in low- and high-elevation catchments (Figures S2 and S3) are also modest, resembling those in medium elevations.

These increases follow the expectation that a moistened atmosphere associated with climate warming will promote intensified precipitation extremes [60,61]. Differences between elevation zones are likely to arise from other factors, including orographic features [24] and storm types [6].

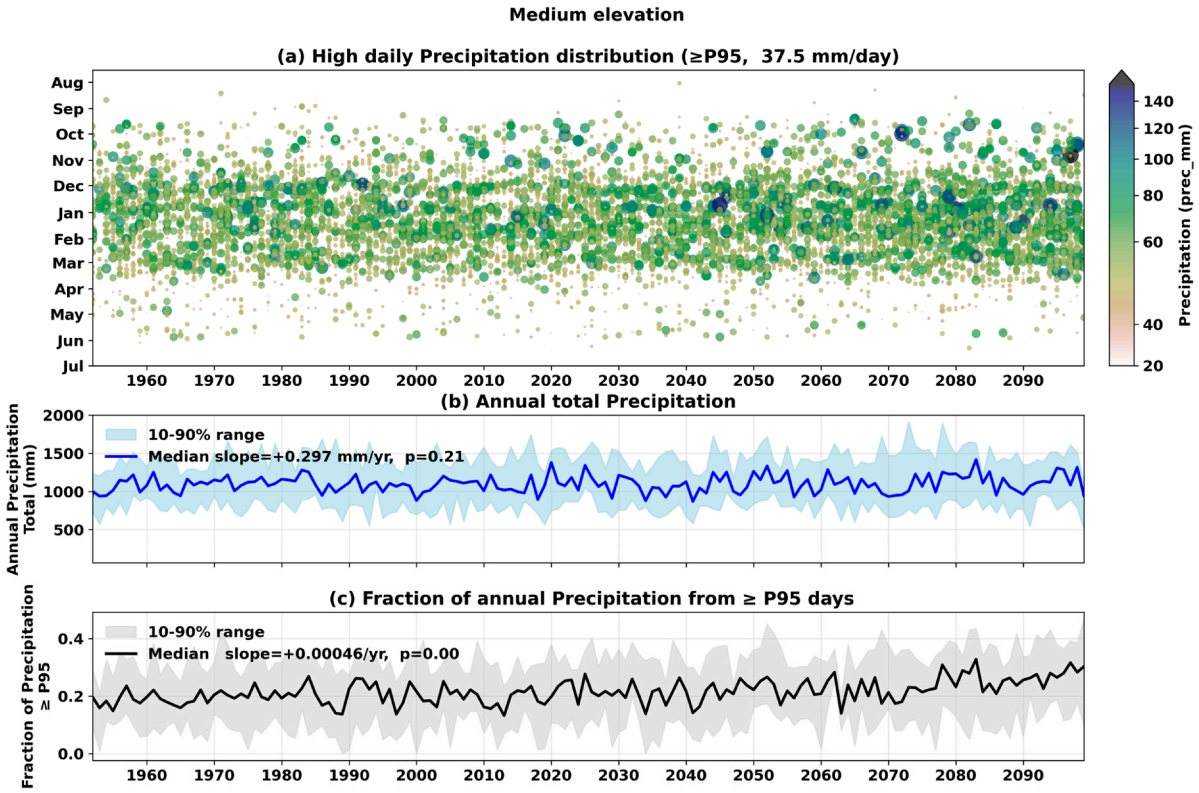


Figure 4. Time series (1952–2099) of precipitation measures for all of the 13 downscaled CMIP simulations for medium-elevation catchments. Upper panel (**a**) shows all days, from all 13 models, whose precipitation reaches or exceeds the P95 threshold (≥37.5 mm day^{-1}). Months on *y*-axis plotted from August to July so the winter wet season is centered. Daily amounts are denoted by color and dot size, so that higher daily values appear as larger, darker dots. Middle panel (**b**) shows annual total precipitation, where thick blue curve is the median and the shaded band covers the 10–90% range of 13 model values. Lower panel (**c**) shows fraction of each year's precipitation contributed by P95 daily events, where thick black line is median and shaded band covers the 10–90% range of 13 model values. Linear trend and associated p-value significance of annual total median and P95 fraction median are annotated on middle and lower panels.

3.3. Runoff Variation and Changes

Annual runoff variability varies considerably from year to year (Table A1), with standard deviation registering 46% of its annual mean during the 1952–2014 historical period for the Delta Watershed, in accord with coefficients of variability of observed annual streamflow records presented in Dettinger et al. [62]. In comparison, the standard deviation of annual precipitation over the Delta Watershed is 28% of its historical mean. Contributions to annual totals from high-percentile precipitation and runoff days both vary greatly. But, the high-percentile daily runoff varies even more so than analogous precipitation measures. The standard deviation of historical P95sum/year is 69% of its mean value, and that of Q98sum/year is much larger, 143% of its mean. And, while P95 yearly counts vary with a standard deviation of 3 days/year, Q98 counts in the historical period vary with a standard deviation of more than 10 days/year (Table A1). Echoing the strong influence of heavy daily precipitation on observed annual precipitation totals [11] Q98sum/year correlates strongly ($r = 0.86$) with Delta Watershed Qann. This correlation is not quite as high as that for the nonheavy runoff $Q < 98$ ($r = 0.95$; Table S4), but it is nonetheless remarkable since the Q98 fraction constitutes only, on average, 10% of the Qann runoff in the historical period. Q98sum/year vs. Qann correlations distributed across individual catchments (Figure 5) show that Q98 influences on interannual runoff fluctuations during the historical period are

greatest in low- and medium-elevation catchments, and that this influence tends to increase during the future period, likely reflecting the increased occurrence and overall volume of Q98 events. In contrast (Figure 5), Q98sum/year vs. Qann correlations are lower in most of the high-elevation catchments, and future-period correlations decline across several of them, likely reflecting diminished numbers and volume contributions of Q98 events in high-elevation catchments during the future period (Table 3). Together, the changes in correlation indicate how future interannual runoff variation in the Delta Watershed tends to be more strongly influenced by high-percentile daily runoff events from low and medium elevations and less strongly by that from high elevations. Pearson correlations reported in this paragraph and the one below are well above the two-tailed critical 0.01 significance value of 0.325 for 60 degrees of freedom.

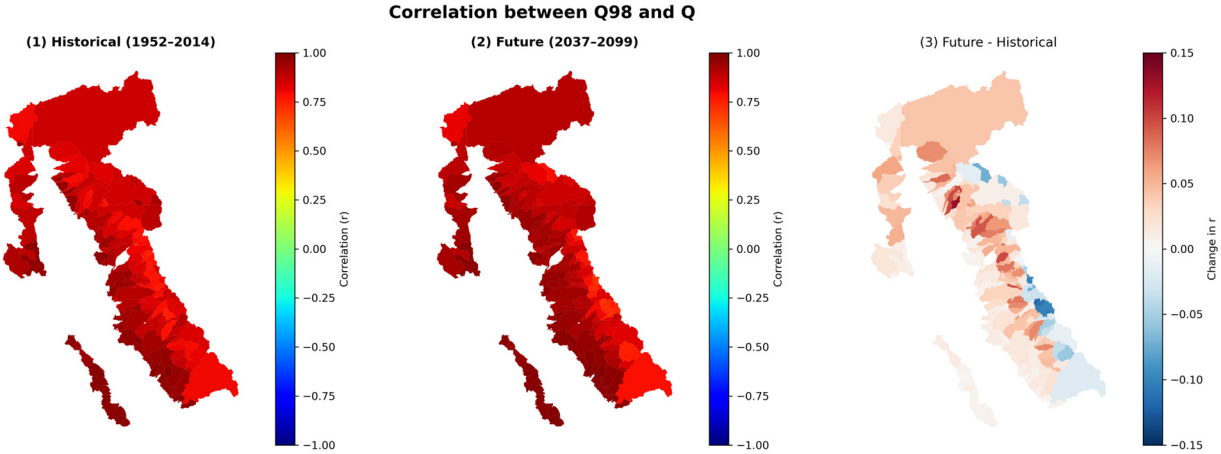


Figure 5. Correlations, Q98 sum/year vs. Qann, for each catchment during the historical period and during the future period, along with future–historical differences.

Table 3. Daily extreme event threshold values, historical (1952–2014) period, for Delta Watershed, low-, medium- and high-elevation catchments. Values are mean of individual model percentile amounts +/− standard deviations calculated from 13 individual SSP370 model projections. P95 and P99.9 thresholds are percentiles of historical wet days ($p \geq 1$ mm). P10y and P30y values are determined from all daily values for 30-year return period. Q thresholds are determined from all historical daily values. Units in millimeters.

Metric	Whole Basin	Low	Medium	High
P95	35.55 ± 1.35	30.67 ± 0.89	37.48 ± 1.52	45.69 ± 1.45
P99.9	76.63 ± 3.79	60.88 ± 4.51	82.59 ± 4.49	101.91 ± 4.09
P30y	83.71 ± 4.10	65.29 ± 4.78	91.09 ± 6.10	113.25 ± 5.27
Q98	5.77 ± 0.21	4.71 ± 0.17	6.99 ± 0.29	9.38 ± 0.60
Q99.9	15.76 ± 1.59	14.11 ± 0.93	20.67 ± 2.16	15.96 ± 1.02
Q30y	27.26 ± 3.69	22.88 ± 3.17	35.57 ± 5.26	22.54 ± 3.42

Unsurprisingly, variations in Q98sum/year cumulative annual runoff volume are associated with variations in P95sum/year contribution to annual precipitation volume. Individual catchments exhibit P95sum/year vs. Q98sum/year correlations ranging from 0.6 to 0.9 (Figure S4), and the overall aggregate Delta Watershed correlation is 0.79 over the historical period (Table S4). In the future period, P95sum/year vs. Q98sum/year correlations increase, with the Delta Watershed-level correlation rising to 0.84, and, with the exception of some high-elevation catchments, correlations of individual catchments also increase (Figure S2). This linkage between Q98 and P95 is further illustrated by charting

their level of variability over the historical through 21st Century future period (Figure S5), showing the close match of a sinuous low-frequency increase in variability for the Delta Watershed and the low- and medium-catchment subsets. But, in high-elevation catchments, while the interannual variability of P95 precipitation events also increases, the variability of high-percentile runoff (Q98) diminishes steadily. The pattern of increased P95sum/year vs. Q98sum/year over most of the Delta Watershed demonstrates the increasing direct linkage between high-percentile daily precipitation and high-percentile daily runoff as high-percentile precipitation events amplify and climate warms. Diminished correlations in some of the high-elevation catchments demonstrate how runoff is modified by surface hydrological processes and precipitation forms (rain vs. snowfall), wherein the magnitude of variability does not necessarily translate from event-scale precipitation to event-scale runoff. This is addressed below.

Thus, although annual mean precipitation increases only marginally and annual runoff is essentially unchanged in the projections, in most catchments, there is a decided increase in the occurrence of high-percentile runoff days (Table A1 and Figure 6), echoing similar findings from prior-generation CMIP5-projected meteorological forcings in a different, more spatially resolved, hydrological model applied to the nearby Lake Tahoe basin [63]. The VIC-projected Q98 days rise from 7.3 to 12.5 days/year from the historical to the future period (Table A1). Also, the Q98sum/year contribution to cumulative annual runoff more than doubles, from 9.4% to 19.8%, on average. Over the Delta Watershed, the increased proportion of Q98 runoff derives from the increased number of Q98 events and a modest 8.4 mm to 9.6 mm increase in intensity, determined from their annual total volume divided by their annual number of days. The increasing weight of Q98 events is also expressed as a greater influence on Delta Watershed annual runoff variation, wherein the Q98sum/year vs. Qann correlation rises to 0.90 (Table S4 and Figure 5) while the non-heavy runoff Q < 98sum/year vs. Qann correlation drops to 0.88 (Table S4 and Figure S6).

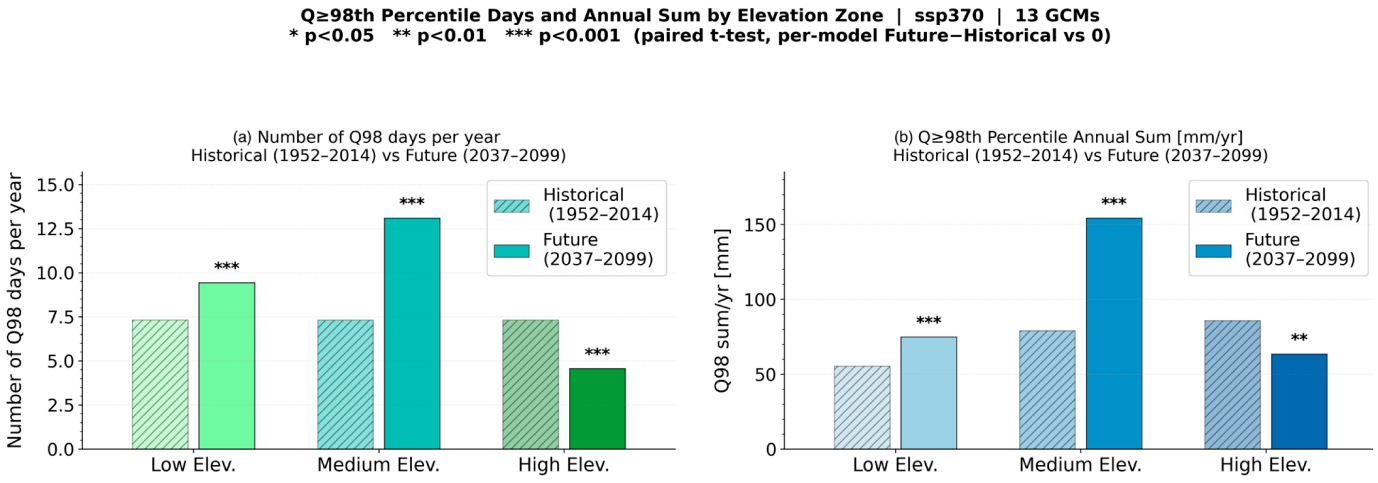


Figure 6. (**a**) Q98 occurrences (days/year; green)and (**b**) Q98sum/year cumulative volume (in millimeters; blue) in 1952–2014 historical (hatched) and 2037–2099 future (solid) periods for low- (lightest color), medium- (intermediate color) and high-elevation (darkest color) catchments. Cases having *p*-values of future-minus-historical differences across the 13 simulations that fall below 0.05, 0.01 and 0.001 significance levels designated by asterisks.

Notably, in the historical period, while the annual fraction of total precipitation contributed by P95 daily precipitation events increases somewhat from low (18%) to high elevations (22%), the annual fraction of total runoff contributed by Q98 daily runoff events declines quite markedly, from about 17% in low elevations to about 8% in high elevations. This decline reflects the effects of snow in damping high-intensity precipitation events, as it

stores water volume that later is more gradually released as snowmelt. However, as warming advances and snow accumulation diminishes, high-percentile runoff characteristics change. Q98 events exhibit increased numbers in low and medium elevations but decreased numbers in high elevations (Figure 6). Future period shifts in the historical period distributions of daily runoff for each of the elevational zoned sets of catchments (Figure S7a–d) help to explain the differences. Rainfall catchments produce greater volume from Q98 daily extremes than snow dominated catchments, which store precipitation rather than generating immediate runoff, with later snowmelt events being more spread out in time than the shorter-period storm-generated rainfall runoff. Overall, the Delta Watershed Q98 number of days in 2037–2999 increases to 170%, and Q98sum/year volume increases to 192% of its historical levels (Table A1). This rise in frequency and volume is explained by increases in these measures in low- and especially medium-elevation catchments (Table A1). Low and medium elevations exhibit Q98 increases (Table A1 and Figures 7–9), with Q98 annual counts up to 9.4 days/year and 13.1 days/year from their historical average of 7.3days/year, and Q98sum/year rising to 135% and 195% of historical average runoff volumes. In low and medium elevations, future-period correlations of Q98sum/year with Qann totals increase to higher levels than in the historical period (Table S4 and Figure 5).

In contrast to increases in low and medium elevations (Figures 7–9) and in spite of increases in high-elevation P95 events, future high-elevation Q98 occurrences decrease to 4.6 days/year from 7.3 days/year (Table A1 and Figure 6). Q98 accumulated volume falls slightly to 7% of the annual total from its historical fraction of the annual total at 8%. Q98sum/year volume falls to 74% of its historical level, which helps to explain the previously noted weakening of high-elevation future Q98 variability (Figure S5). And, although there is a noticeable increase in extremely high winter runoff events (Figure 10a), correlations of Q98sum/year vs. Qann volumes in several of the high-elevation catchments decline (Figure 5).

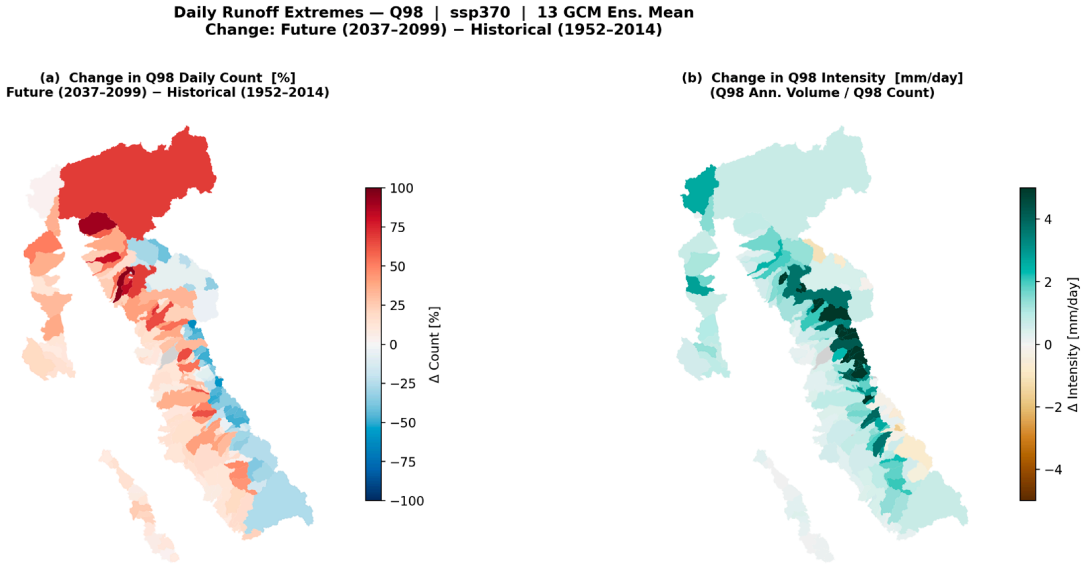


Figure 7. Changes, future (2037–2099) minus historical (1952–2014), in (**a**) Q98 numbers (%) and (**b**) Q98 intensity (in millimeters). Changes are the average difference in counts or intensities from 13 model simulations.

Across catchments, future (2037–2099) vs. historical (1952–2014) changes in occurrence and changes in intensity of Q98 days are shown in the maps of Figure 7. Low- and medium-elevation catchments exhibit increases in Q98 intensity of 1 mm/day to more than 4 mm/day. Furthermore, in low and medium elevations, future Q < 98 volumes fall to 84%

and 79% of their historical levels, and their correlations with annual runoff weaken somewhat (Figure S4). In high-elevation catchments, Q98 events and volume contributions do not exhibit future increases, and in some cases decline, a point that will be discussed below.

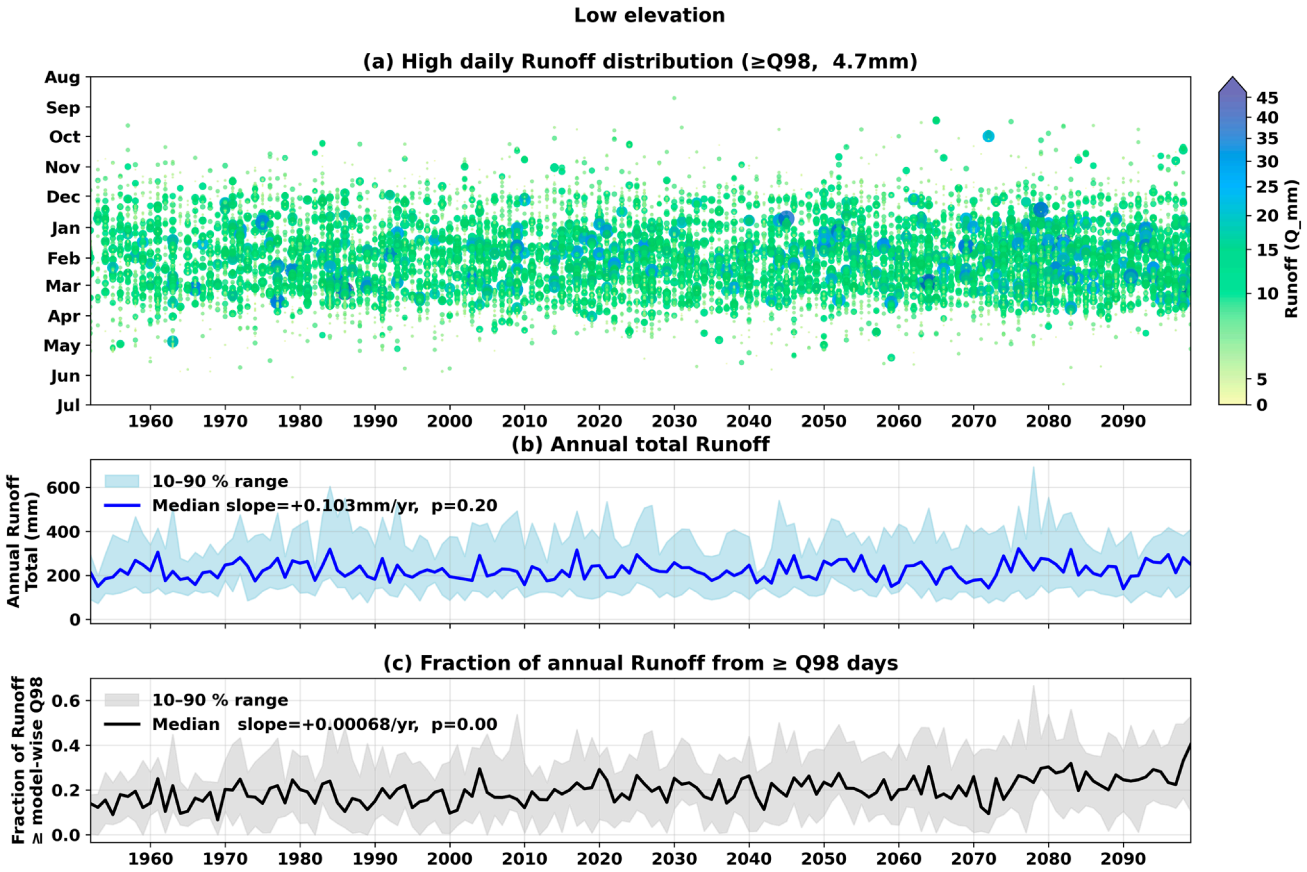


Figure 8. For 13 VIC–CMIP6 model projections in low-elevation catchments, (**a**) daily Q98 runoff events where dot size and color intensity represent daily magnitude), (**b**) annual runoff and (**c**) fraction of annual runoff contributed by Q98 days. In (**b**,**c**), heavy lines show median, and shading shows 10% to 90% of 13 model projections.

A more resolved description of the temporal structure of low-elevation Q98 changes (Figure 8) shows how occurrences of high-runoff days increase from the mid- to late-21st Century, with the largest gains in January–March and a pronounced rise in the 2070s–2080s. Annual runoff totals exhibit a slight, non-significant upward trend over 1952–2099. By contrast, the contribution of the most intense events grows markedly: the fraction of annual runoff arising from Q98 days (≥4.7 mm day^{-1}) increases significantly, from 17% in the historical period to about 23% in the future period. The low-elevation catchments are rain-dominated, and the strengthening of daily runoff extremes is mostly driven by heavier daily precipitation extremes. Collectively, the results indicate a future in which short-duration runoff exerts a growing influence relative to water-year means in low-elevation parts of the Delta Watershed (Figure 8). Notably, even stronger increases occur in medium-elevation catchments, shown by a similar census of Q98 occurrence in Figure 9. Here, the fraction of annual runoff arising from Q98 days (≥7.0 mm day^{-1}) increases to about double that of low-elevation catchments, from 11% in the historical period to 24% in the future.

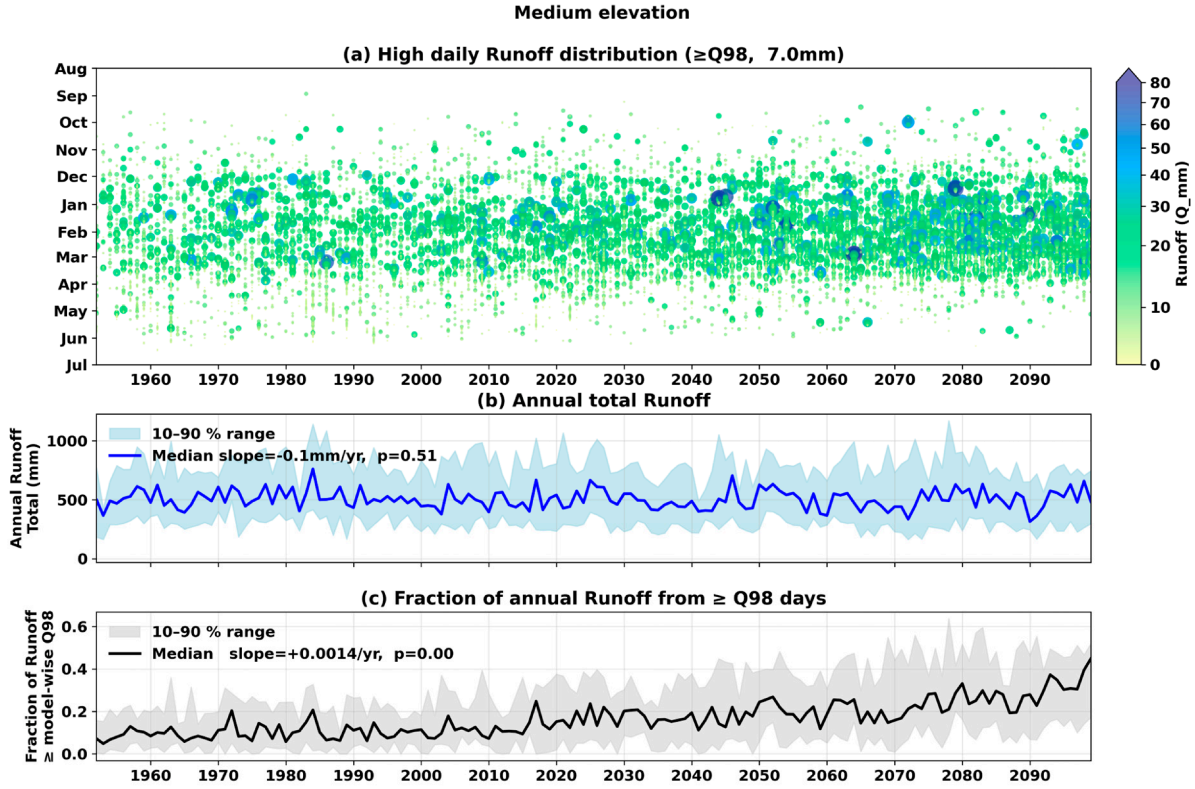


Figure 9. As in Figure 8 but for medium-elevation catchments.

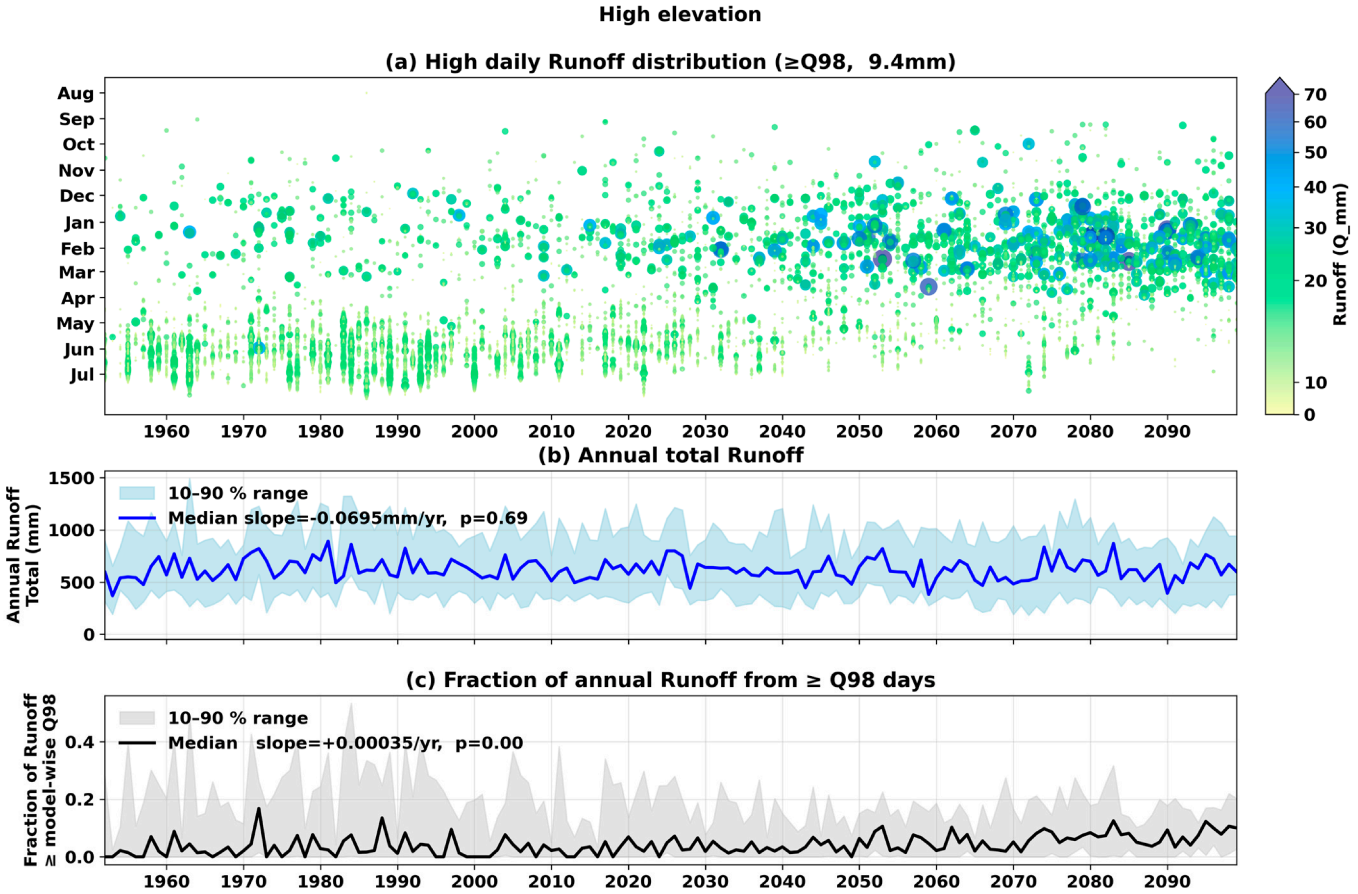


Figure 10. As in Figure 8 but for high-elevation catchments.

Snow vs. rain tradeoffs appear to be at the root of the Q98 declines in the highest-elevation catchments where historical Q98 events largely derive from spring snowmelt surges (Figure 10). These analyses indicate that changing 21st Century snowmelt patterns diminish Q98 contributions from high-elevation catchments. As implied by Figure 3, much of the future daily runoff population shifts to lower mean runoff in earlier months as the seasonal SWE profile (Figure S8) diminishes. Prior to the 2040s, the high-elevation runoff time series features flows from distinct populations of winter storms and early-summer snowmelt peaks (Figure 10), whereas after the 2040s, those snowmelt-driven spikes largely disappear, replaced, to an extent, by an increase in wintertime high-runoff days that become most prominent after the 2080s. In areas where spring snowmelt surges are the source of most/all of the annual Q98 episodes, the climate change-induced declines in SWE (Figure S8) sap the amount of snow available to melt into Q98 episodes, reducing their scale, means and annual variations. Thus, future warming diminishes the historically high, late spring–early summer runoff snowmelt pulses in favor of earlier-season, but mostly lower-amplitude, runoff pulses in the future.

3.4. Wet-Year vs. Dry-Year Ingredients

On an interannual basis, precipitation in California varies to a greater degree than elsewhere in the United States [62,64], with several noteworthy dry years and wet years in recent decades (https://wrcc.dri.edu/my/climate/tracker/CA accessed 2 April 2026). Years falling into the wettest third (i.e., "wettest years") and driest third (i.e., "driest years") of the historical period provide telling examples of the importance of high-intensity daily precipitation and runoff days. Considering P95 days within the Delta Watershed over the historical record (Figure 11 and Figure S9, and Table S4), the wettest years yield, on average, 7.4 P95 days that account for 26% of the total annual precipitation in those years. This compares to the driest years, which contain only 2.1 P95 days that account for only 13% of annual precipitation. The contrast in high-percentile runoff is even greater, with wettest-third years having 16.6 Q98 days that contribute 17% of annual total runoff and driest years having only 1.2 Q98 events that contribute 3% of annual total runoff. The future period yields an even larger gulf between wet and dry years. The wettest years in 2037–2099 yield, on average, 8.3 P95 days, accounting for about 30% of the total wettest-year precipitation, compared to the driest years, which yield only 2.5 P95 days that account for only 16% of annual precipitation. Remarkably, Q98 fractional contributions to annual Delta Watershed runoff double in the future for all three (dry, normal and wet) year classes. The strong increase in heavy-runoff contributions in wet years would present greater challenges in managing flood flows, wherein the increased runoff volume in wet years has an even greater proportion delivered by high-percentile daily events. A consequence is that the wet year increase carries through to very high, flood-potential, daily precipitation and runoff events, discussed below in Section 3.5.

Differences in wettest year vs. driest year numbers of Q98 runoff days are even more striking (Figure 11b) than the heavy P95 precipitation day counts (Figure 11a). Mean annual runoff itself, of course, is much greater in wet years, wherein wet years from the historical period produce, on average, 743 mm/year runoff, 2.7 times as much as the dry year average of 269 mm/year. In the projections, there are modest declines in annual runoff. For the historical period, the wettest years averaged 743 mm of runoff compared to dry years with only 269 mm. Future wet years generate 708 mm compared to dry years, which generate 239 mm (Table S4). For all three annual precipitation classes, future years have relatively larger increases in Q98 days and their volume contributions. Future wettest years exhibit a strong increase, 24 days/year compared to 16 days in the historical period. These future wettest years contribute 31% of wettest-year total runoff, compared to future driest

years whose 2.5 Q98 days contribute 8% of driest-year total runoff. The future increase in the Delta Watershed Q98 fraction is provided disproportionately by low- and medium-elevation catchments (Figure 7) in wet years (Figure 11). In contrast, Q98 contributions in high-elevation catchments in the wettest years decline considerably due to fewer future Q98 days/year. But importantly, as discussed below in Section 3.6, very-high-percentile runoff in high elevations exhibits increases that actually exceed those in medium elevations. In an era where water supplies are increasingly dear, intensified Q98 incidence and heightened annual contributions in low- and medium-elevation catchments during wet years underscore the need for programs such as Forecast Informed Reservoir Operations (FIRO; [65]) and FloodMAR [66], which aim to save or store water generated in storm events.

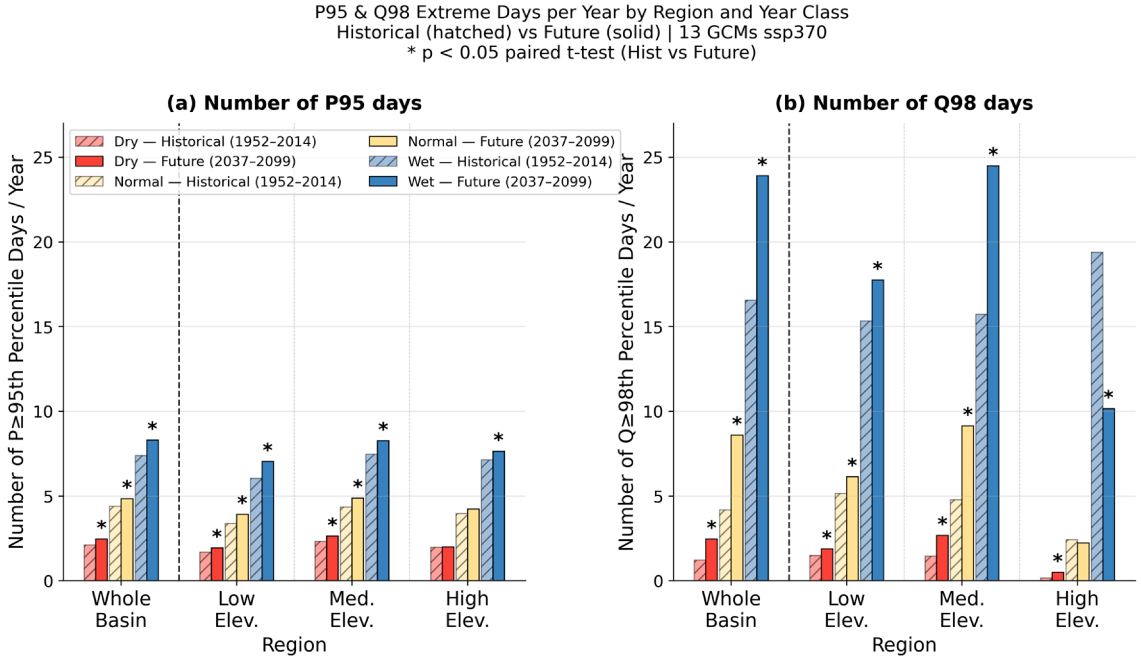


Figure 11. For Delta Watershed and low-, medium-, and high-elevation catchments, (**a**) the number of P95 days/year and (**b**) the number of Q98 days/year in 1952–2014 historical (hatched) and 2037–2099 future (solid) periods. Cases having p-values of future-minus-historical differences across the 13 simulations that fall below 0.05, 0.01 and 0.001 significance levels are designated by asterisks.

3.5. Seasonality of Runoff Changes

A monthly census of progressively higher-percentile daily runoff episodes reveals some of the seasonal dynamics that govern the changes. In the low-elevation catchments (Figure S10), there is relatively little change in monthly total runoff, but consistent with increases in extreme precipitation events, there are significant increases in high-percentile runoff. These future monthly occurrences register the same seasonal pattern as those in the historical period, reflecting the primarily rainfall-sourced runoff in low elevations. Runoff event increases across the 21st Century are seen in December through March, and the relative changes in the 9th percentile and especially the 99.9th percentile eclipse the occurrences in the historical period.

For medium-elevation catchments, seasonal shifts in Q98 and Q99.9 runoff days (Figures S11 and S14) are greater than those in low-elevation catchments. Historical medium-elevation monthly mean as well as Q98 and Q99.9 runoff exhibit increased volumes in the December-through-March winter period and diminished volumes in spring and early summer from April–June (Figures S11 and S14). By late 21st Century, winter-month Q98 and Q99.9 days double compared to historical levels (Figure S11). Also noteworthy is

that counts of Q98 and Q99.9 of the aggregated model runs show an increase from early (1952–1981) to the later (1991–2020) periods, already occurring even during this historical period, evidently in response to rising temperatures (Figure S16).

The high-elevation catchments undergo large changes in runoff seasonality. Monthly mean runoff shifts become higher in December–February and lower in May–July (Figures 12 and 13), reflecting the demise of snow water storage and later-season snowmelt and a compensating increase in rainfall and earlier snowmelt. Seen in Figure 13, Q98 occurrences in July, June and May are prominent from 1955 through about 2040, but fade thereafter, while Q98 occurrences in November through March become more frequent, beginning in about 2030 and strengthening over the ensuing decades. Q99.9 runoff exhibits strong increases in winter months. In medium-elevation catchments (Figure 14), Q98 occurrences in April, May and June decline considerably as warming advances during the 21st Century, and Q98 numbers in winter and early spring grow higher. In low-elevation catchments, reductions in Q98 spring occurrences (Figures S10 and S12) are most obvious in April and May, but Q98 numbers in February and March increase over the 21st Century.

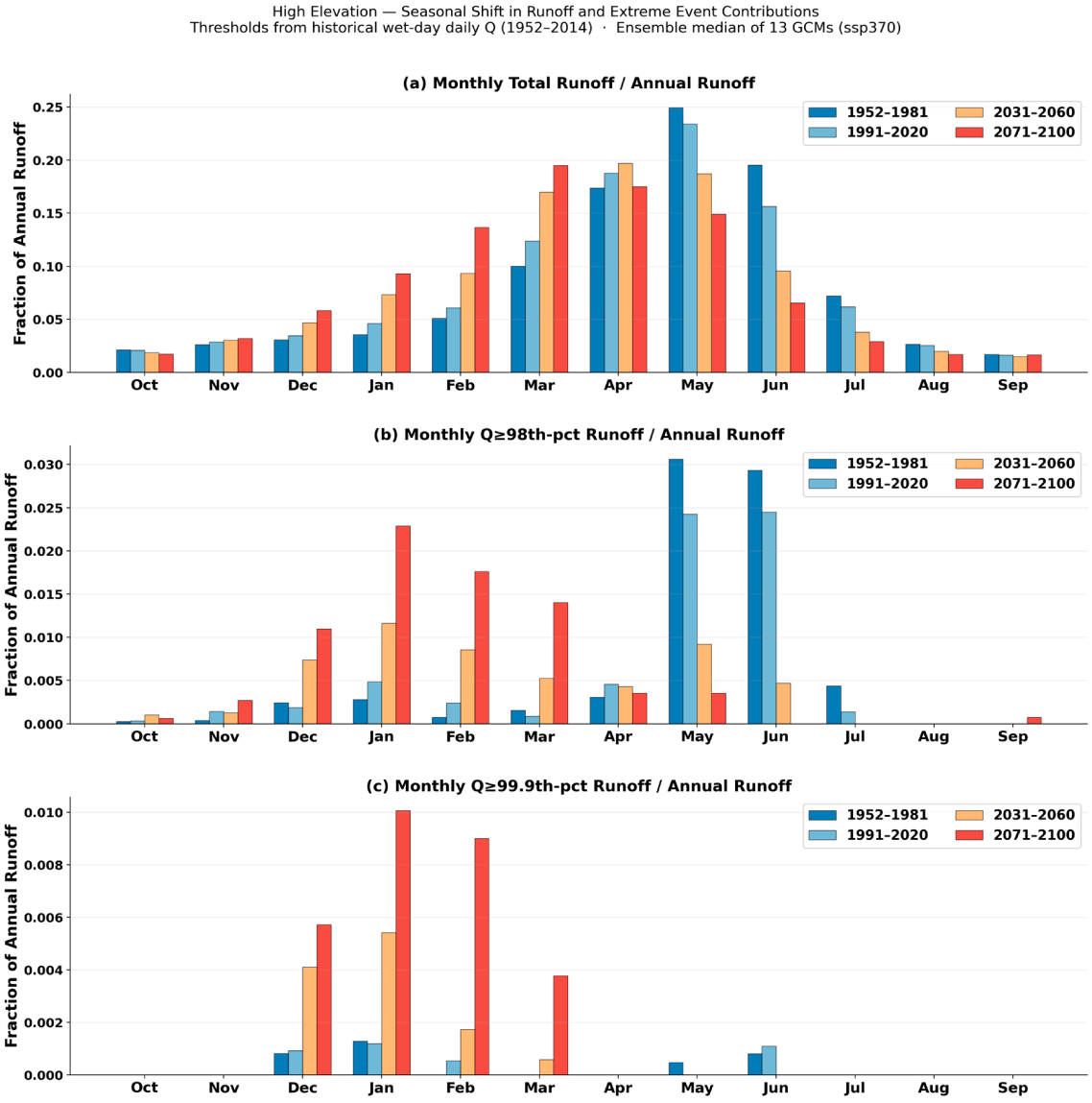


Figure 12. High-elevation catchments, October-September (**a**) monthly mean, (**b**) Q98 runoff volume as fraction of annual, and (**c**) Q99.9 volume as fraction of annual for early historical (dark blue), late historical (light blue), mid 21st Century (orange), and late 21st Century (red) periods.

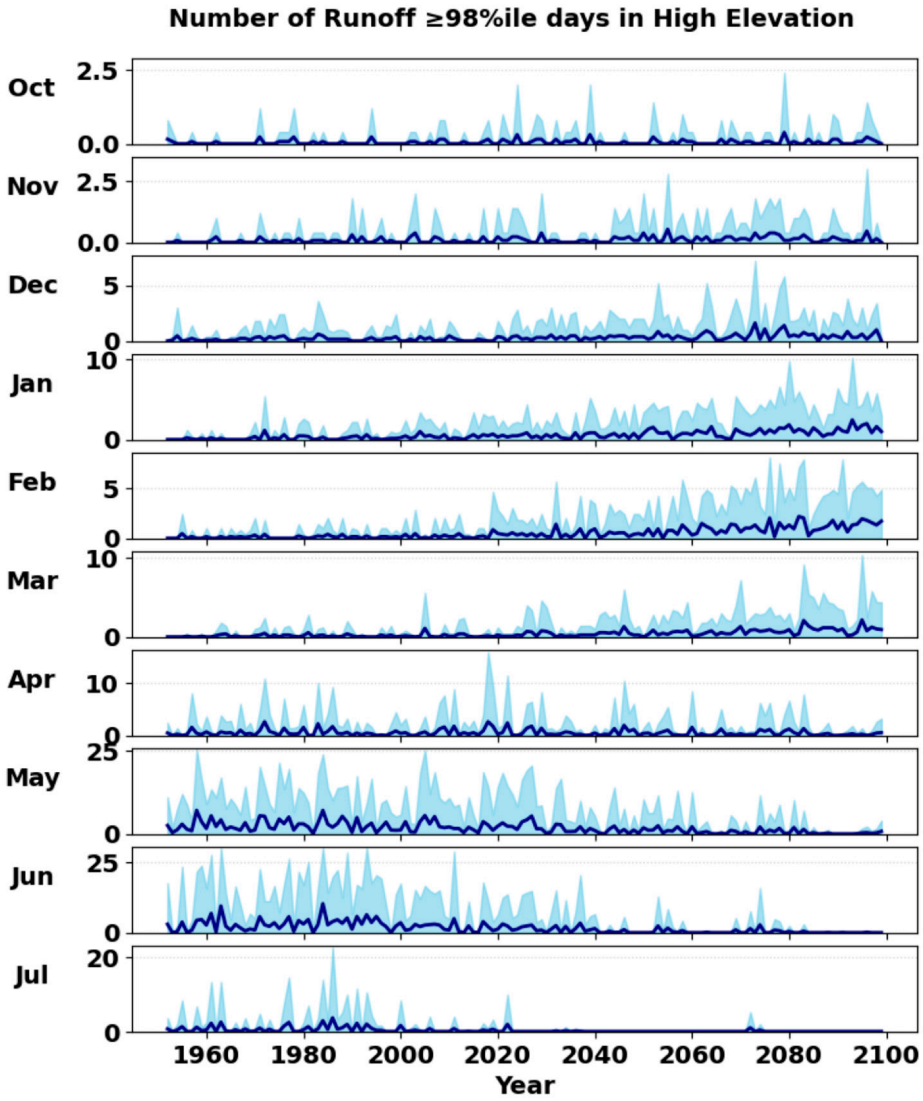


Figure 13. Time series (1952–2099) of the number of Q98 days each year for high-elevation catchments averaged from the set of 13 VIC CMIP6 projections, for each month from October (top) to July (bottom). Mean counts, of 13 projections, shown as solid black line. The 5th through 95th percentiles of modeled Q98 for each year shown by blue envelope.

3.6. Potential Flood Events

Historically, the Delta Watershed has experienced high-magnitude floods [67–69]. Previous studies [2,17] indicate that high-runoff events will intensify as climate changes evolve toward heavier precipitation and diminished snowpacks. Here, considering the Delta Watershed as a whole, the number of high-intensity runoff events increases considerably in the 2037–2099 future period (Figure 15). Overall (Table A1), future period P99.9 and P30y occurrences double and nearly triple, and Q99.9 and Q30y occurrences triple and more than quadruple. P99.9 contributions increase from 1.5% in the 1952–2014 historical period to 2.4% of Pann in the 2037–2099 future, while the Q99.9 contribution increases from 1.0% to 3.6% of Qann. And, as might have been expected, Figure 15 shows that rare high-precipitation and rare high-runoff events tend to align with anomalously wet years, also shown in Table S4 future and historical correlation heatmaps. Increases in numbers and intensity of Q99.9 extremes in the individual catchments are greater in nearly all but the highest of the high elevation catchments, as mapped in Figure S17 and quantified in elevation zones in Table A1. Despite having decreased Q98 extreme counts and annual

volume contributions, the increases in numbers of Q30 extremes and annual volumes are decidedly greater in high-elevation catchments than those in low and medium elevations, e.g., future Q30y counts rise by more than eight times their historical occurrence; i.e., a historical 30-year return period event becomes, on average, a 2.5-year event (Table A1).

These variations in heavy runoff events reflect variations and changes in annual precipitation. Another property that is not considered here is that heavy runoff is often likely to persist over more than one day and may also associate with clusters [70] of extreme storms. Figure 12 shows that in wet (annual precipitation falling within 70th–90th percentile) years, future Q99.9 average counts burgeon to more than 0.6/year from historical counts of little more than 0.1/year, and the standard deviation of future Q99.9 counts, over all years, is nearly double its mean value (Table A1). A similar pattern of changes is found for the even more rarely occurring Q30y events. Future rates of extremely high runoff (Q99.9 and Q30y) occurrence are aligned with, and exhibit similar or even higher magnitude than, the changes in high-intensity precipitation runoff (P99.9 and P30y), also shown in Figure 15. Future increased Q99.9 and Q30y numbers in wet years register as highly significant ($p < 0.001$), more so than the increased P99.9 and P30y numbers in wet years. This underscores the role played by wet years in contributing to the overall change in heavy-runoff events and probably also reflects the importance of heavy events in creating wet years. Importantly, raising water management concerns, this increase in Q99.9 and Q30y would represent a substantial increase in floods.

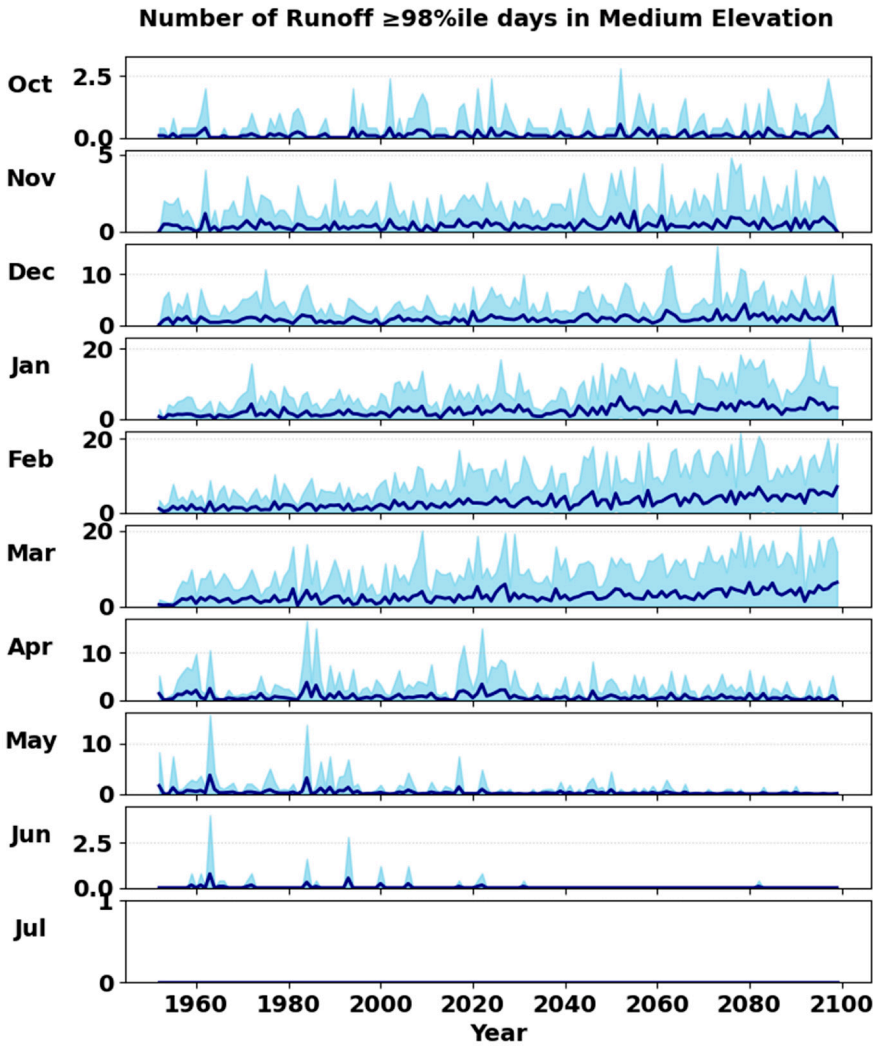


Figure 14. As in Figure 13 but for medium-elevation catchments.

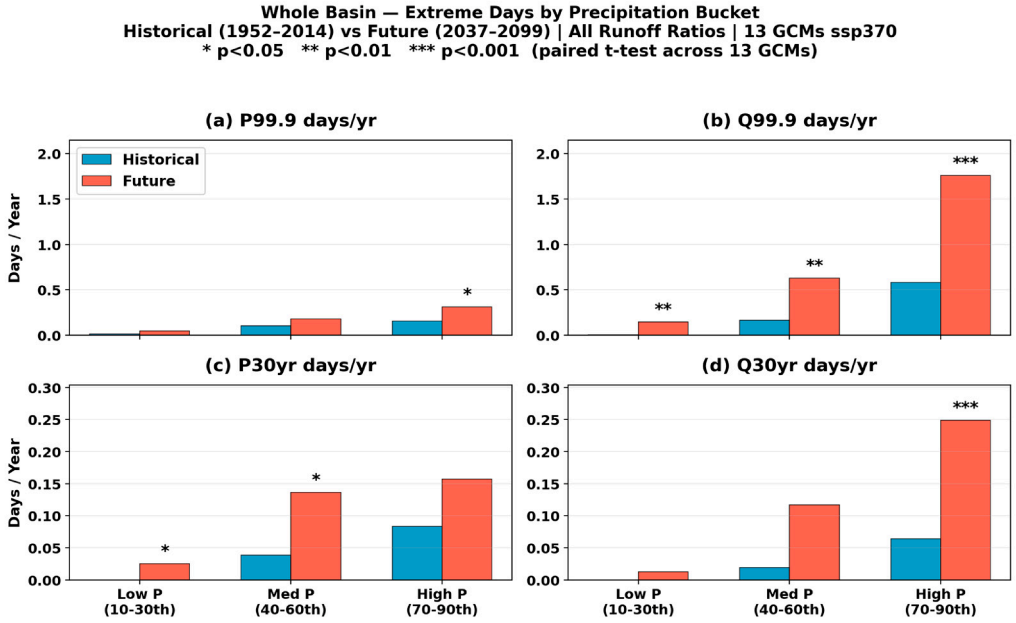


Figure 15. For whole Delta Watershed, mean yearly number [days/year] of high-intensity precipitation days (**a**,**c**) and runoff days (**b**,**d**), historical (blue) vs. future (red) across 13 SSP 370 simulations, at or exceeding 99.9th historical percentile (**a**,**b**) and 30-year historical return period (**c**,**d**), and stratified by annual precipitation (10–30th, 40–60th, and 70–90th historical percentiles). Cases having p-values of future-minus-historical differences across the 13 simulations that fall below 0.05, 0.01 and 0.001 significance levels are designated by asterisks. Note different scales in plots (**c**,**d**) from plots (**a**,**b**).

Even though high-elevation catchments register future reductions in Q98 occurrences, this elevation zone rivals medium- and low-elevation catchments in having significant increases in the occurrence of Q99.9 and Q30y events. This increase comes in the form of increased occurrence of very large winter runoff events, shown in the upper panel of Figure 10 and the Q99.9 time series in Figure S15. Increases can also be seen in the daily runoff future vs. historical distributions shown in Figure S7 and quantified in Table A1. And, while high-elevation Q99.9 contributions are less than those from medium elevations (22 mm vs. 29 mm, respectively (Table A1)), for the even more rarely occurring Q30y events, the future high-elevation annual volume (12.6 mm) exceed that from medium elevations (7.3 mm).

Temperatures on the days experiencing different levels of high-percentile precipitation provide important insight into changes in runoff from higher elevations. The average temperatures for all elevation zones during P99.9 days and during P95 days exhibit steady rises over the historical-through-21st-Century period that are commensurate with the rise in annual mean temperature (Figures S13–S15). In high-elevation catchments over the entire period, the mean Q99.9-day temperature is warmer, by 1 °C to 2.5 °C, than that on P95 days. Temperature series for low- and medium-elevation catchments and for the Delta Watershed (Figure S16) are similarly warmer for P99.9 days than for P95 days. In California's mountainous terrain, the heaviest orographic precipitation advantage is most often delivered by storms having enhanced westerly flow (Dettinger et al. 2004 [24]), as opposed to more northwesterly flows. Confirming expectations, the present results indicate these storms are warmer, are able to carry more water vapor, and thus have elevated freezing levels [62] Thus, as the 21st Century progresses, future high-intensity high-elevation runoff events "retreat" into the core winter months of December through March (Figure S15), very likely the product of warmed and enriched atmospheric river events [3,6,11] and enhancements from rain-on-snow conditions [32]. Correspondingly, from a survey of Q99.9 changes at individual catchments (Figure 16), we find that the lower portions of the

high-elevation catchments experience most of the increase in rare extreme-runoff events, indicating that the highest of the high-elevation catchments are too cold to generate high winter-storm runoff.

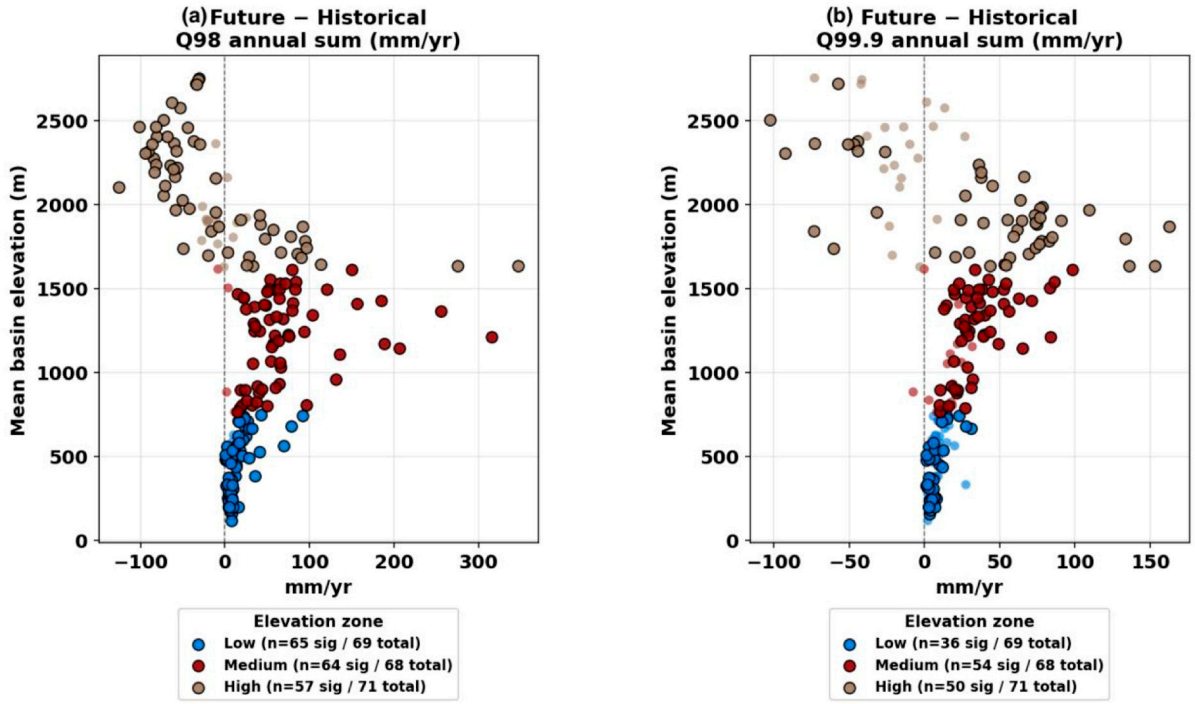


Figure 16. Thirteen-model mean change [%], future (1952–2014) minus historical (1952–2014) Q98sum/year (left) and Q99.9sum/year contribution to annual volume, plotted according to mean elevation (in meters) of each catchment. Blue, red, taupe color dots for catchments in low, medium and high elevation zones. Catchments having *p*-values of future-minus-historical changes across the 13 simulations that fall below 0.05 significance levels are designated by larger, outlined dots.

4. Discussion: The Crucial Role of Medium Elevation Catchments

Notably, in viewing future changes in heavy daily precipitation contributions for each individual catchment, P95sum/year changes in nearly all catchments are positive (Figure S18). However, changes in Q98sum/year and Q99.9 sum/year cumulative runoff volume contributions present a much more complex profile (Figure 16). The heavy daily runoff contributions in intermediate-elevation catchments exhibit the strongest positive changes, in contrast to low-elevation catchments showing smaller positive changes and the higher high-elevation catchments showing negative changes. As indicated by the historical mean hydrographs in Figure 3, medium-elevation catchments are perched in the mixed snow and rain zone that previous studies [18,23,25,27] have shown to be highly sensitive to snow loss and runoff shifts from climate warming.

Q98sum/year changes in medium elevations are decidedly positive, falling between smaller positive changes in low elevations and mixed changes in the lower portion of high-elevation catchments. Q98sum/year future-minus-historical changes in catchments above 1800 m reverse to negative—the negative changes in these higher catchments produce the aggregate negative change in the high-elevation third of the catchments found previously, as in Table A1 and Figure 6. Changes in Q99.9sum/year (Figure 16b) are also universally positive in medium elevations. Increasingly positive Q99.9sum/year changes occur from the surface to about 1600 m, above which changes are mixed from highly positive to negative. Q99.9sum/year changes in the lower portion of high-elevation catchments are mostly positive, but become predominately negative in the highest elevations above 2100 m.

Due to higher baseline temperatures and minimal snow accumulation, low-elevation catchments respond with limited sensitivity to warming-induced shifts in snow-to-rain runoff generation. Low-elevation catchments begin (historically) with the highest fraction of Q98 runoff contributions of all elevation zones and become depleted of snowpack early in the warming progression of the 21st Century (Figure S8). Thus, the low-elevation runoff increases are mostly limited to the increases bestowed by increased precipitation extremes.

In medium-elevation catchments, mean temperatures on P95 days (Figure S16) begin their trajectory through the 1952–2099 model projections at about 2.5 °C and warm to more than 6 °C by 2099. Associated with this and the overall warming, April 1 SWE in these medium-elevation catchments declines to little more than one-quarter of its historical average (Figures S8 and S19, and Table A1) and snow/rain elevations rise by several hundred meters. This indicates that a considerable portion of (formerly) winter-early spring snowfall transitions into rainfall with resulting rainfall runoff and snowmelt runoff. Along with this transition, the large increases in daily runoff events in medium-elevation catchments are likely bolstered by increased rain-on-snow events [71].

Historically, high-elevation catchments have rarely been warm enough for rainfall to occur but may increasingly experience rain-on-snow during warm atmospheric rivers as climate warms, as indicated by warming on P95 and P99.9 days (Figure S16) and supported by rising snow altitudes in recent decades found in observational datasets [32]. P95 day temperatures in the high-elevation catchments, although warming similarly as medium-elevation catchments, are cooler by about 4 °C. High-elevation catchments have had considerably more snow (Figure S6) and, under projected warming hydrographs that historically included the most high-intensity runoff in spring and early summer, progressively shift toward lower-amplitude runoff earlier in the season (Figures 3, 10 and 14). This shift mutes enough runoff events at levels below the historical 98th percentile threshold (Figure S7c) so that the number and volume of Q98 events decline through the early to late-middle 21st Century, reaching essentially an end-of-century low as early as about 2070. For the highest of the high-elevation catchments, the annual number of Q98 events decline in frequency and in their annual cumulative runoff, in response to losses of their historically large snow-water storage. These highest, coldest catchments contain a higher proportion of winter and spring snow-covered area than the lower high-elevation and medium-elevation catchments, which are warmer and closer to the mixed snow/rain temperature band.

The difference between medium-elevation catchments and high-elevation catchments is further shown by a chronology of SWE changes associated with heavy runoff events, compiled yearly through the course of the historical through future period. A revealing long-term transition of event-specific SWE change is shown by the time series of the 13-model outcomes plotted in Figures 17 and 18. The generally high degree of significance in trends of the 13-model median SWE change is shown by Mann–Kendall p-value statistics annotated in Figures 17 and 18, and reinforced by a census of individual model trends along with t-test of the 13-member set of trends in Table S5. In medium-elevation catchments, throughout the historical and future periods, the 13-model median change in SWE that occurs during Q98 events is significantly positive, indicating that these events are sufficiently cool enough that they manage to accumulate snow. Snow accumulation and cool temperatures indicate that their occurrence is mostly in winter and early spring (Figures 9 and 13). In this case, the amplitude of the accumulation diminishes through the 21st Century, reflecting unabated warming (Figure S16) that leads to higher snow levels and greater rain and less snow accumulation. The time series of medium-elevation Q99.9 SWE change (Figure 17) exhibits a similar downward trend, but by 2030, the SWE change approaches zero, indicating that storms are warm enough (Figure S16) that they produce greater rainfall and much less snow accumulation.

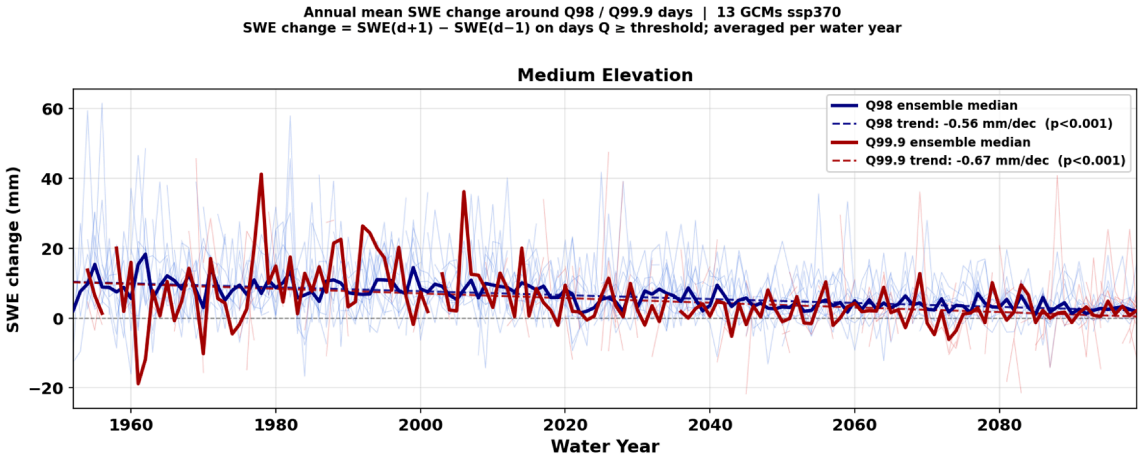


Figure 17. Annual average of SWE change (in millimeters), day after minus day before Q98 runoff events (blue) and Q99.9 events (red) for medium-elevation catchments. Dark lines show median of 13 individual VIC-CMIP6 model results. Linear trends (in millimeters/decade) are shown by dashed lines and slopes, and significance listed in annotation. Blanks in time series reflect years lacking Q99.9 events across the 13-model dataset.

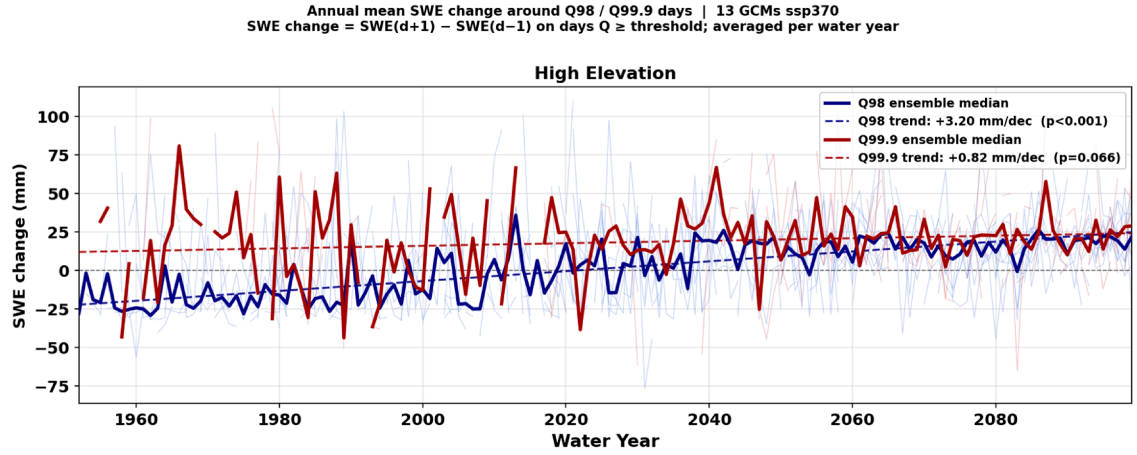


Figure 18. As in Figure 17 but for high-elevation catchments.

In contrast to medium elevations, the high-elevation 13-model annual median Q98 SWE change (Figure 18) in the historical period and that in the early future period are significantly negative. These negative SWE changes represent snowmelt-driven runoff events that occur most commonly during the earlier decades of the record in spring and summer, as shown in Figures 9 and 14. Importantly, during the decades after 2040, the high-elevation annual aggregate Q98 SWE change shifts to positive, reflecting winter storm events (Figures 10 and 14) whose air temperatures must be cooler than those in historical spring and summer runoff surges but warmer than winter storms were during earlier decades. This transition is consistent with the demise of spring and summer SWE (Figure S6) and the shift of the high-elevation hydrograph toward earlier runoff (Figure 3). The result is a loss of the relatively large spring–summer snowmelt runoff events that, in turn, drives the reduction of Q98 events in higher-elevation catchments. Heavier Q99.9 runoff events exhibit more volatility (Figure 18), with relatively high positive-SWE-change episodes throughout the 1952–2099 time history, and the trend of the median SWE change does not meet the $p < 0.05$ significance criteria. Positive SWE changes indicate storm events that are cold enough to accumulate snow but still warm enough to generate heavy concurrent daily runoff. The calendar of runoff events in the high-elevation zone shown in the top panel of Figure 18

demonstrates that the heaviest events nearly always occur within December and March, coincident with the season of heightened North Pacific storm activity.

The time series in Figure 10, Figure 18 and Figure S14 indicate that, as climate warms, high-percentile daily runoff events in high-elevation catchments shift more and more to resemble that which historically occurred at medium elevations. There is a marked transition from the more unimodal (spring-dominated Q98) runoff of the historical period toward the bimodal historical mid-zone hydrograph, under climate warming. The mechanisms that yield high-altitude Q98s evolve considerably over the course of the 21st Century. By late century, winter precipitation-driven Q98s, rather than spring and summer snowmelt Q98s, become the dominant mode of high-percentile runoff, resembling medium-elevation historical runoff pulses as shown in Figures 9 and 13.

Thus, the changes in high-percentile runoff shown in Figure 16 indicate that the medium-elevation catchments along with a few of the lowest high-elevation catchments are the zones of greatest extreme-runoff change in the Delta Watershed, providing the greatest increase in days when runoff reaches or exceeds the historical 98th percentile. Importantly, these medium-elevation catchments constitute nearly half of the area of the Delta Watershed, as well as contributing about half of its annual runoff, and thus are crucial for both water resources and the generation of Delta Watershed-wide flood flows.

Importantly, in the historical period, the high-percentile (P95) fraction of annual precipitation is relatively high and increases from low (0.18) to high elevations (0.24), listed in Table A1. In contrast, for high-percentile runoff (Q98) events, average annual volume fractions decrease with elevation, from low (0.17) to medium (0.11) to high elevation (0.08). This decline is an indication of how snow processes mute the extremes in precipitation. However, as climate warms, snow accumulation declines, so this damping effect is diminished in the medium-elevation (historically mixed rain-snow) zones.

In low elevations, the future Q98 fraction of annual runoff rises to 0.23, an increase of 33%. But in medium elevations, the Q98 fraction rises considerably more, from 0.11 to 0.24 (Table A1), an increase of 108%. This difference suggests an index of hydroclimate change that might complement the often-used April–July fraction of runoff (M. Roos, [25]) can be obtained to monitor the heavy runoff activity. An index consisting of the ratio of medium-elevation Q98 fract/annual runoff to low-elevation Q98 frac/annual runoff, is shown in Figure 19. The low-elevation fraction is employed as the denominator, so that it is the comparative standard against which medium-elevation fractional changes are gauged. Low-elevation Q98 fractional contributions are employed because they are almost entirely generated by changes in storm-rainfall totals as expressed by rainfall runoff, increases are moderate in magnitude, and they change quite steadily over the nearly 150-year projections. This rainfall-driven change is compared to the medium-elevation Q98 changes, which reflect mostly the changing rain-snow and SWE-persistence changes there. Projections of this index (Figure 19) undergo a steady rise (in the midst of expected interannual variation) in the ratio of medium-elevation to low-elevation Q98 fraction, from a level of about 0.6 in the historical period to approximately 1.0 in the future period, reflecting the transition of the historical middle-elevation hydroclimatology and hydrology into essentially the equivalent of historical low-elevation conditions. Guided by the mean of the individual projections in this sample set, the trend in the ratio begins to level off by about 2080, indicating that medium-elevation heavy runoff and flood generation will likely become mostly rainfall-dominated, similarly to the low-elevation catchments. Considering the entire 1952–2099 time series, upward trends are found for each of the individual GCM hydrology projections, ranging from about 0.02/decade to 0.06/decade, all of them at a high level ($p \leq 0.02$) of statistical significance (Table S6).

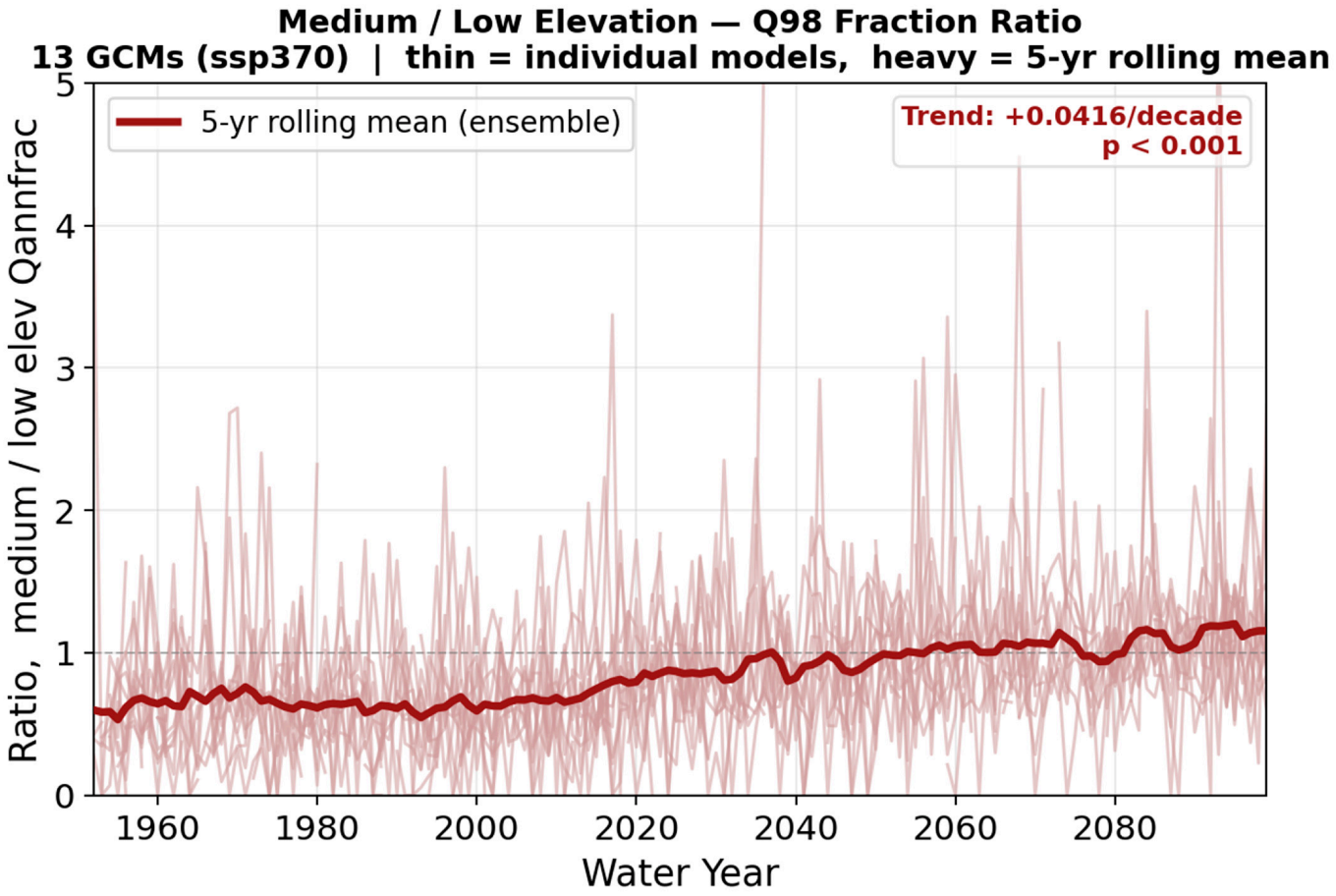


Figure 19. Ratio of Q98 fractions of annual runoff, medium-elevation to low-elevation catchments of the Delta Watershed. Light lines are ratios from VIC simulations of 13 individual GCMs, dark heavy line is ensemble mean of individual model ratios smoothed with 5-year running mean.

5. Conclusions

Although projected annual precipitation volumes are relatively unchanged, the intensification of heavy precipitation events is a clear signal in the modeled climate future for California. The possible shift toward a more volatile future precipitation regime has attracted a considerable body of research, but climate change-driven heavy runoff events have received less attention. This study therefore investigates how climate model-projected warming and storm intensifications might change future high-percentile daily-runoff events from the varied catchments that drain into California's Sacramento and San Joaquin Delta. The focus here is daily runoff extremes and their aggregated annual contributions in 210 catchments within the Sacramento/San Joaquin Delta Watershed. The study employs VIC hydrological model simulations developed from 13 LOCA downscaled 1950–2100 SSP370 CMIP6 projections.

As expected, with warming and intensified daily precipitation, high daily-runoff events aggregated over the Delta Watershed are increased in number and volumes, and contribute increasingly to annual total runoff. A finer-scale perspective, however, reveals considerable differences in heavy runoff changes across low-, medium- and high-elevation catchments. These differing runoff changes exhibit a growing fingerprint of event-scale hydroclimate change.

Runoff events in low elevations are primarily rainfall-dominated. Future (2037–2099) events exhibit a moderate, 29% increase in frequency and a 36% increase in the cumulative volume they contribute, driven almost entirely by increasing frequency and annual volume

contributions of high-percentile precipitation. Low-elevation runoff events continue to occur primarily in winter months, in alignment with heavy precipitation events.

Medium-elevation catchments have historically been sufficiently cool enough to accumulate snow but are close enough to freezing levels that future warming produce substantial shifts to rain instead of snow. So, medium-elevation catchments play a leading role, beginning in the early 21st Century, in generating enhanced runoff events, more so than from low- and high-elevation catchments. Increased frequency and volume of extreme-runoff events contributed by medium-elevation catchments contribute more, per unit area. In medium-elevation catchments, the number of future Q98 days rises to 1.8 times their historical rates of occurrence, and their cumulative volume burgeons from 15% to 29% of annual total runoff. Timing of medium-elevation events shifts so they are solidly occurring in winter months. And, since they constitute nearly half of the area and more than half of the total precipitation and runoff of the Delta Watershed, the extreme contribution from medium-elevation catchments amounts to considerably more total volume.

High-elevation catchments, which have historically supplied spring and summer snowmelt-fed runoff events, begin a marked shift after about 2040 in the SSP370 scenarios as the climate warms and the amount of spring and summer snow-left-to-melt diminishes in future decades. This transition results in a runoff regime that increasingly resembles that of historical medium-elevation catchments with winter rainfall runoff and rain-on-snow-fed high runoff signatures and fading spring and summer snowmelt events. Thus, Q98 daily runoff events shift profoundly in the 2037–2099 future period. Because there is less snow remaining to melt, late-spring and early-summer events that occur commonly in the historical record largely disappear by mid-21st Century, while earlier spring and winter events become more numerous. Q98 events in these high-elevation catchments experience declines in numbers and their cumulative volume falls to 74% of its historical level. However, for more extreme cases, represented by Q99.9 and Q30y threshold events, the high-elevation catchments exhibit marked increases, with frequency and annual aggregated volume contribution increasing more than three-fold. These heightened runoff events mostly occur in November through March, quite likely driven by exceptionally warm and productive winter storms.

As in observations, the interannual variability of high daily precipitation in the Delta Watershed is high with coefficients of variation of 0.28 (historical period) and 0.29 (future period) aggregated over the 13 individual model projections employed here. Corresponding variability of heavy daily runoff events and their contribution to annual total runoff is even higher. From the 13 individual VIC projections, the standard deviation of annual cumulative Q98 runoff reaches 100% and more of its overall mean volume. Importantly, year-to-year fluctuations of these heavy daily runoff events exert a somewhat stronger influence on interannual runoff totals in the future. Most of the increase in high-runoff events occurs in years when the cumulative precipitation volume is normal or, especially, wet. In the historical record, daily Q98 runoff counts in wet years are nearly 14 times as frequent as in dry years, and cumulative Q98sum/year (volume per year contributions) is almost 15 times greater than in dry years. Very-high-percentile runoff events exceeding Q99.9 thresholds increase in all three elevation zones, even at high elevations. These heavy runoff days, which probably would be flood events, are likely driven by extreme precipitation produced in warm storms. Runoff days reaching or exceeding historical 10-year and 30-year return-period thresholds arrive four to six times as often in future decades.

Further work is needed. This study interrogated changes in heavy runoff by tallying daily events reaching or exceeding selected threshold levels. Many daily events are members of multi-day episodes, and it would be useful to conduct further analysis of multi-day events. Since runoff events are influenced by prior wetness or dryness, it would be useful

to consider initial conditions such as soil moisture status. The present results are drawn solely from a VIC-modeled SSP370 single-member ensemble of CMIP6 projections, which may present a distorted set of outcomes, so comparative analyses of projected runoff from other hydrological models, more GCM ensemble members and other SSPs will be useful to investigate and compare results. It seems likely that much of the heavy precipitation and associated runoff is driven by atmospheric rivers [3,6,62], but the heavy runoff associations might be more closely investigated. Most of our analysis of future hydrological conditions is based on 2037–2099 aggregate measures, but this should be parsed into shorter future periods in future research. This study focused mostly on Delta Watershed and elevation-zone totals, but future studies should also evaluate routed runoff and hydrological variation within and between the many catchments that compose the Delta Watershed, along with the many possible effects they might have on the management of water resources, hazards and ecosystems. Exploration of similar or contrasting changes in other mountainous catchments would provide further insights.

Resource and flood managers and operators of California's Sierra Nevada reservoirs, which are nearly all sited in medium and low elevations and draw their inflows from the full range of high to low elevations, will need to manage heightened and more frequent high flows. The present study demonstrates significant differences among the future contributions of streamflow and flood-generation processes from the various elevation zones. Downstream of major reservoirs, the Sacramento/San Joaquin Delta water resources, conveyances, and ecosystems will need to contend with these changing and increasing flood flows, along with rising sea levels and aging levees. Challenges will arise from changes in flood flows from all three elevation zones and will require management strategies that accommodate the differing changes in all three elevation zones. These challenges are a clear example of the urgency of California planning to improve the State's resilience to future storms and flooding. The planning efforts are outlined in a growing array of planning and programmatic awareness efforts and are increasingly looking toward the potential value of forecast-informed reservoir operations (FIRO), a strategy that places increased reliance on modern improvements in weather forecasting skill days to weeks in advance, to better manage flood risks while also increasing the robustness of the State's major water supplies. Additionally, California's Flood-Managed Aquifer Recharge (Flood-MAR) efforts aim to exploit high-flow events to replenish groundwater supplies by directing the runoff onto suitable agricultural lands, working landscapes, and managed natural areas where it can safely infiltrate into aquifers. Finally, monitoring changing flood and resource contributions from medium-elevation catchments, in comparison to those from low elevations, could be a useful metric for tracking the progress of changes in hydroclimate extremes over the Delta Watershed.

Supplementary Materials: The following supporting information can be downloaded at: https://www.mdpi.com/article/10.3390/w18212702/s1, Table S1: VIC vs. CDEC Validation Metrics; Table S2: CMIP6 GCMs, regionalized using LOCA2 hybrid statistical/dynamical process; Table S3: Metrics by Dry/Wet/Normal Year Class; Table S4: Pearson correlation heat maps, whole Delta Watershed, between annual time series of several hydrometeorological measures; Table S5: Significance tests, $\mathrm{SWE}(d+1) - \mathrm{SWE}(d-1)$ centered on Q98 and Q99.9 runoff days; Table S6: Trend of the ratio: medium elevation Q98 annual fraction/low elevation Q98 annual fraction; Figure S1: 9 Sierra basins employed in monthly and annual VIC validation in Table S1; Figure S2: 13 VIC–CMIP6 model projections of precipitation in low elevation catchments, Figure S2: 13 VIC–CMIP6 model projections of precipitation in high elevation catchments; Figure S4: Correlation between the annual accumulations, P95 sum/yr vs. Q98 sum/yr; Figure S5: Running standard deviations of P95 annual sum and Q98 annual sum standard deviation; Figure S6: Correlations of <Q98 sum/yr vs. Qann; Figure S7: Density of daily runoff [mm/d] occurrences during 1952-2014 historical and 2037–2099 future for low-elevation, medium-elevation, high-elevation catchments and the whole Delta Watershed; Figure S8: Mean snow

water equivalent (SWE) through the water year in low, medium, and high catchments and whole Delta Watershed; Figure S9: For whole Delta Watershed, (a) average number of P95 days/year and (b) Q98 days per year, (c) average fraction of annual total precipitation contributed by P95 days, and (d) annual total runoff contributed by Q98 days for dry, normal and wet years; Figure S10: Low elevation catchments, (a) October-September monthly mean, (b) Q98 and (c) and Q99.9 daily runoff occurrences for historical, mid 21st Century, and late 21st Century periods; Figure S11: Medium-elevation catchments, (a) October-September monthly mean, (b) Q98 and (c) and Q99.9 daily runoff occurrences for historical, mid 21st Century, and late 21st Century periods; Figure S12: Time series (1955–2095) number of Q98 days each year for low elevation catchments averaged from the set of 13 VIC CMIP6 projections, for each month from October to July; Figure S13: Time series (1955–2095) of number of Q99.9 days each year for low elevation catchments averaged from the set of 13 VIC CMIP6 projections, for each month from October to July; Figure S14: Time series (1955–2095) of number of Q99.9 days each year for medium elevation catchments averaged from the set of 13 VIC CMIP6 projections, for each month from October to July; Figure S15: Time series (1955–2095) of number of Q99.9 days each year for high elevation catchments averaged from the set of 13 VIC CMIP6 projections, for each month from October to July; Figure S16: Annual mean temperature (red), annual average temperature of days having P95 precipitation events (blue), annual average temperature during days having P99.9 precipitation events (orange) aggregated over (a) whole basin, (b) low elevation, (c) medium elevation, and d) high elevation catchments; Figure S17: Changes, future (2037–2099) minus historical (1952–2014) in (a) Q99.9 numbers [%] and (b) intensity; Figure S18: Changes, future (2037–2099) minus historical (1952–2014) P95sum/yr for each catchment, plotted according to their mean elevation; Figure S19: Multi-model time series of April 1 SWE [mm] for medium elevation catchments.

Author Contributions: Conceptualization, L.S. and D.R.C.; Methodology, L.S., D.R.C., D.W.P., M.D.D. and M.P.; Software, L.S., D.W.P. and B.B.; Validation, L.S.; Formal analysis, L.S. and B.B.; Investigation, L.S., D.R.C., D.W.P., B.B., M.D.D., A.G. and M.P.; Resources, D.R.C., A.G. and M.P.; Data curation, L.S., D.W.P. and B.B.; Writing—original draft, D.R.C.; Writing—review and editing, L.S., D.R.C., D.W.P., B.B., M.D.D., A.G. and M.P.; Visualization, L.S., D.R.C. and M.P.; Supervision, D.R.C.; Project administration, D.R.C.; Funding acquisition, D.R.C. and A.G. All authors have read and agreed to the published version of the manuscript.

Funding: This research was supported by the California Energy Commission under the ECP-20-006 award and by the University of California Multi-Campus Research Programs and Initiatives "Just Transitions" project, the University of California Climate Action Initiative through the COEQWAL project, the California Department of Water Resources' AR Program, and the US Department of the Interior via the Southwest Climate Adaptation Science Center (SW CASC, host award G24AC00611).

Data Availability Statement: The LOCA2 downscaled CMIP SSP370 meteorological projections employed and the associated VIC hydrological simulations over the California region are available from the CalAdapt Analytics Engine, https://analytics.cal-adapt.org/.

Acknowledgments: We thank Peter Yao for calculations and Dennis Lettenmaier for discussions.

Conflicts of Interest: The authors declare no conflicts of interest.

Appendix A

Thirteen GCMs (ssp370) Historical: 1952–2014, Future: 2037–2099, Mean and Std Dev shown as separate columns per elevation zone. Std dev is ensemble mean of 13 per-model inter-annual std dev of annual values within each model, ddof = 1), P95/P99.9 thresholds: historical wet days ($p > 1$ mm)|Q98/Q99.9: historical Q > 0 days, P10y/P30y: All historical daily P (exactly 10/30-year return periods, Q10y/Q30y: derived from all historical daily Q. Annual fraction measures are averages of annual fractions of individual years and models, and differ from fractions of overall accumulations aggregated across years and models. Bold future measures designate statistically significant difference from historical measure via paired t-test on 13, per-model means, $p < 0.05$.

Table A1. Annual and Daily P, Q, T and SWE Statistics.

Variable	Mean				Interannual Std				Intermodel Std			
	WholeBasin	Low	Medium	High	WholeBasin	Low	Medium	High	WholeBasin	Low	Medium	High
Tann (deg C) (Hist)	10.30	14.86	9.96	6.27	0.707	0.668	0.722	0.739	0.101	0.092	0.106	0.102
Tann (deg C) (Fut)	13.47	17.84	13.19	9.54	1.04	0.990	1.06	1.06	0.585	0.524	0.620	0.584
Pann (mm/yr) (Hist)	1011	738.9	1100	1129	287.2	224.7	303.0	345.5	22.49	17.60	21.69	30.61
Pann (mm/yr) (Fut)	1036	766.0	1132	1141	298.8	236.9	316.1	355.9	38.17	30.43	38.17	48.94
SWEapr1 (mm) (Hist)	193.2	8.60	162.5	443.1	121.9	8.34	115.8	268.6	35.72	2.12	35.68	72.41
SWEapr1 (mm) (Fut)	78.39	1.16	44.85	221.7	63.62	2.17	46.50	170.5	19.42	0.432	12.75	54.12
Qann (mm/yr) (Hist)	492.0	239.0	539.9	668.5	225.8	130.7	248.7	301.7	25.81	11.69	24.00	46.45
Qann (mm/yr) (Fut)	476.3	246.8	520.7	635.3	226.3	136.4	246.7	301.8	30.96	17.49	31.73	47.63
Q snowfraction (Hist)	0.381	0.088	0.354	0.631	0.061	0.034	0.069	0.071	0.015	0.009	0.016	0.018
Q snowfraction (Fut)	0.240	0.037	0.205	0.449	0.066	0.024	0.070	0.091	0.027	0.007	0.025	0.050
Q rainfraction (Hist)	0.619	0.912	0.645	0.369	0.061	0.034	0.069	0.071	0.015	0.009	0.016	0.018
Q rainfraction (Fut)	0.760	0.963	0.795	0.551	0.066	0.024	0.070	0.091	0.027	0.007	0.025	0.050
TduringP95days (deg C) (Hist)	3.73	8.67	3.46	−0.715	1.73	1.92	1.75	2.05	0.546	0.421	0.518	0.641
TduringP95days (deg C) (Fut)	6.20	10.94	5.93	1.95	2.25	2.17	2.21	2.65	0.671	0.578	0.607	0.825
P95 count/yr (Hist)	4.62	3.70	4.71	4.36	3.03	2.59	3.03	2.93	0.168	0.132	0.173	0.153
P95 count/yr (Fut)	5.39	4.56	5.48	4.75	3.29	3.03	3.29	3.06	0.561	0.524	0.675	0.459
P95 sum/yr (mm) (Hist)	217.6	145.4	236.0	267.8	148.9	105.1	158.6	188.6	3.54	3.61	3.41	7.31
P95 sum/yr (mm) (Fut)	261.5	185.0	284.1	301.2	168.3	126.5	180.1	204.7	24.02	21.07	30.59	27.03
P95 frac/annualP (Hist)	0.199	0.181	0.199	0.217	0.102	0.100	0.100	0.113	0.004	0.006	0.004	0.004
P95 frac/annualP (Fut)	0.233	0.222	0.234	0.242	0.108	0.111	0.107	0.117	0.015	0.020	0.021	0.016
P<95 count/yr (Hist)	87.60	70.09	89.37	82.66	15.57	14.20	15.58	14.96	3.14	2.49	3.29	2.90
P<95 count/yr (Fut)	84.06	66.71	85.85	80.12	15.26	13.58	15.51	15.29	3.17	2.16	3.11	3.48
P<95 sum/yr (mm) (Hist)	773.7	578.8	847.1	844.6	186.3	155.4	197.4	217.4	21.15	15.74	20.72	25.64
P<95 sum/yr (mm) (Fut)	755.2	566.8	830.8	822.5	183.0	150.8	196.9	213.2	19.04	20.61	25.77	28.71
P<95 frac/annualP (Hist)	0.780	0.797	0.784	0.766	0.098	0.097	0.097	0.110	0.004	0.005	0.004	0.004
P<95 frac/annualP (Fut)	0.746	0.758	0.750	0.742	0.105	0.107	0.105	0.114	0.016	0.020	0.022	0.016
P99.9 count/yr (Hist)	0.099	0.079	0.101	0.095	0.326	0.285	0.337	0.311	0.007	0.000	0.008	0.000
P99.9 count/yr (Fut)	0.202	0.193	0.209	0.175	0.481	0.447	0.491	0.430	0.103	0.131	0.076	0.078
P99.9 sum/yr (mm) (Hist)	8.24	5.25	9.21	10.67	27.18	18.91	30.88	34.85	0.415	0.304	0.589	0.307
P99.9 sum/yr (mm) (Fut)	17.82	13.11	19.90	20.88	42.80	31.09	47.40	52.27	9.42	8.35	7.57	9.42
P99.9 frac/annualP (Hist)	0.007	0.006	0.007	0.008	0.023	0.024	0.024	0.027	0.001	0.001	0.001	0.001
P99.9 frac/annualP (Fut)	0.015	0.014	0.015	0.015	0.034	0.033	0.035	0.039	0.008	0.009	0.006	0.007
P10y count/yr (Hist)	0.111	0.111	0.111	0.111	0.356	0.338	0.352	0.331	0.000	0.000	0.000	0.000
P10y count/yr (Fut)	0.211	0.230	0.220	0.189	0.487	0.481	0.507	0.446	0.102	0.138	0.075	0.091
P10y sum/yr (mm) (Hist)	9.19	7.15	10.03	12.27	29.43	21.86	32.07	36.63	0.385	0.425	0.576	0.359
P10y sum/yr (mm) (Fut)	18.57	15.35	20.81	22.32	43.19	32.87	48.55	53.62	9.36	8.86	7.51	10.45

Table A1. *Cont.*

Variable	Mean				Interannual Std				Intermodel Std			
	WholeBasin	Low	Medium	High	WholeBasin	Low	Medium	High	WholeBasin	Low	Medium	High
P10y frac/annualP (Hist)	0.008	0.009	0.008	0.009	0.025	0.027	0.025	0.029	0.001	0.001	0.001	0.001
P10y frac/annualP (Fut)	0.015	0.017	0.016	0.017	0.035	0.036	0.036	0.040	0.008	0.010	0.006	0.008
P30y count/yr (Hist)	0.048	0.048	0.048	0.048	0.215	0.220	0.225	0.215	0.000	0.000	0.000	0.000
P30y count/yr (Fut)	0.116	0.126	0.116	0.101	0.348	0.357	0.344	0.316	0.070	0.089	0.071	0.059
P30y sum/yr (mm) (Hist)	4.21	3.26	4.60	5.65	19.02	15.07	21.73	25.50	0.202	0.184	0.321	0.175
P30y sum/yr (mm) (Fut)	11.03	9.01	11.95	13.06	33.28	26.11	35.78	41.09	6.90	5.86	7.55	7.74
P30y frac/annualP (Hist)	0.004	0.004	0.004	0.004	0.017	0.019	0.017	0.020	0.001	0.001	0.001	0.001
P30y frac/annualP (Fut)	0.009	0.010	0.009	0.010	0.027	0.028	0.027	0.031	0.006	0.007	0.006	0.006
Q98 count/yr (Hist)	7.32	7.32	7.32	7.32	10.49	7.95	8.85	13.45	0.000	0.000	0.000	0.000
Q98 count/yr (Fut)	12.46	9.43	13.10	4.56	12.33	9.43	12.35	6.82	2.37	1.44	2.12	1.41
Q98 sum/yr (mm) (Hist)	62.18	55.31	79.03	85.89	88.56	67.27	100.6	164.5	3.57	2.20	5.36	5.22
Q98 sum/yr (mm) (Fut)	119.9	74.89	154.3	63.50	129.6	85.43	158.9	92.71	21.45	10.85	23.36	18.82
Q98 frac/annualQ (Hist)	0.094	0.174	0.113	0.083	0.091	0.125	0.099	0.132	0.010	0.006	0.011	0.003
Q98 frac/annualQ (Fut)	0.198	0.232	0.235	0.072	0.139	0.146	0.156	0.078	0.030	0.026	0.029	0.021
Q<98 count/yr (Hist)	357.9	357.9	357.9	357.9	10.48	7.94	8.85	13.45	0.000	0.000	0.000	0.000
Q<98 count/yr (Fut)	352.8	355.8	352.1	360.7	12.32	9.42	12.35	6.82	2.37	1.44	2.12	1.41
Q<98 sum/yr (mm) (Hist)	429.8	183.7	460.9	582.7	158.9	73.16	172.9	200.8	27.76	11.11	27.12	43.11
Q<98 sum/yr (mm) (Fut)	356.4	171.9	366.3	571.8	124.2	62.60	121.0	233.6	21.89	8.84	22.10	45.90
Q<98 frac/annualQ (Hist)	0.906	0.826	0.887	0.917	0.091	0.125	0.099	0.132	0.010	0.006	0.011	0.003
Q<98 frac/annualQ (Fut)	0.802	0.768	0.765	0.927	0.139	0.146	0.156	0.078	0.030	0.026	0.029	0.021
Q99.9 count/yr (Hist)	0.381	0.381	0.381	0.381	1.05	1.01	1.04	1.27	0.000	0.000	0.000	0.000
Q99.9 count/yr (Fut)	1.16	0.668	1.02	0.923	2.02	1.58	1.76	1.59	0.324	0.178	0.333	0.275
Q99.9 sum/yr (mm) (Hist)	7.78	6.78	10.20	7.11	22.60	19.13	29.58	23.16	0.849	0.579	1.12	0.591
Q99.9 sum/yr (mm) (Fut)	25.68	12.35	29.12	22.46	47.05	30.30	53.48	41.99	6.62	3.22	8.41	7.00
Q99.9 frac/annualQ (Hist)	0.010	0.016	0.012	0.007	0.026	0.039	0.032	0.020	0.001	0.001	0.001	0.002
Q99.9 frac/annualQ (Fut)	0.037	0.028	0.038	0.025	0.058	0.057	0.061	0.041	0.009	0.007	0.012	0.007
Q10y count/yr (Hist)	0.111	0.111	0.111	0.111	0.450	0.479	0.490	0.447	0.000	0.000	0.000	0.000
Q10y count/yr (Fut)	0.455	0.245	0.437	0.600	1.04	0.805	0.962	1.23	0.154	0.121	0.186	0.196
Q10y sum/yr (mm) (Hist)	2.92	2.52	3.84	2.52	12.24	11.10	17.41	10.03	0.363	0.316	0.480	0.354
Q10y sum/yr (mm) (Fut)	13.01	5.59	15.53	16.80	30.77	18.44	35.77	36.37	3.92	2.51	5.95	5.37
Q10y frac/annualQ (Hist)	0.004	0.005	0.004	0.003	0.015	0.022	0.018	0.010	0.001	0.001	0.001	0.001
Q10y frac/annualQ (Fut)	0.018	0.011	0.019	0.018	0.038	0.034	0.041	0.036	0.006	0.005	0.008	0.006
Q30y count/yr (Hist)	0.048	0.048	0.048	0.048	0.267	0.265	0.275	0.252	0.000	0.000	0.000	0.000
Q30y count/yr (Fut)	0.219	0.118	0.169	0.401	0.624	0.443	0.522	0.920	0.107	0.080	0.091	0.150
Q30y sum/yr (mm) (Hist)	1.43	1.23	1.89	1.24	8.16	6.85	11.08	6.59	0.201	0.194	0.288	0.198
Q30y sum/yr (mm) (Fut)	7.26	3.05	7.26	12.58	21.49	11.59	23.48	30.51	2.94	2.08	3.49	4.03
Q30y frac/annualQ (Hist)	0.002	0.002	0.002	0.001	0.009	0.013	0.011	0.007	0.000	0.000	0.000	0.000
Q30y frac/annualQ (Fut)	0.009	0.006	0.009	0.013	0.026	0.022	0.026	0.030	0.004	0.004	0.004	0.004

References

1. Polade, S.D.; Gershunov, A.; Cayan, D.R.; Dettinger, M.D.; Pierce, D.W. Precipitation in a Warming World: Assessing Projected Hydro-Climate Changes in California and Other Mediterranean Climate Regions. *Sci. Rep.* **2017**, *7*, 10783. [CrossRef] [PubMed]
2. Swain, D.L.; Langenbrunner, B.; Neelin, J.D.; Hall, A. Increasing precipitation volatility in twenty-first-century California. *Nat. Clim. Change* **2018**, *8*, 427–433. [CrossRef]
3. Gershunov, A.; Shulgina, T.; Clemesha, R.E.S.; Guirguis, K.; Pierce, D.W.; Dettinger, M.D.; Lavers, D.A.; Cayan, D.R.; Polade, S.D.; Kalansky, J.; et al. Precipitation regime change in Western North America: The role of Atmospheric Rivers. *Sci. Rep.* **2019**, *9*, 9944. [CrossRef] [PubMed]
4. Seneviratne, S.I.; Zhang, X.; Adnan, M.; Badi, W.; Dereczynski, C.; Di Luca, A.; Ghosh, S.; Iskandar, I.; Kossin, J.; Lewis, S.; et al. Weather and Climate Extreme Events in a Changing Climate. In *Climate Change 2021: The Physical Science Basis. Contribution of Working Group I to the Sixth Assessment Report of the Intergovernmental Panel on Climate Change*; Masson-Delmotte, V., Zhai, P., Pirani, A., Connors, S.L., Péan, C., Berger, S., Caud, N., Chen, Y., Goldfarb, L., Gomis, M.I., et al., Eds.; Cambridge University Press: Cambridge, UK; New York, NY, USA, 2021; pp. 1513–1766. [CrossRef]
5. Pierce, D.W.; Cayan, D.R.; Das, T.; Maurer, E.P.; Miller, N.L.; Bao, Y.; Kanamitsu, M.; Yoshimura, K.; Snyder, M.A.; Sloan, L.C.; et al. The key role of heavy precipitation events in climate model disagreements of future annual precipitation changes in California. *J. Clim.* **2013**, *26*, 5879–5896. [CrossRef]
6. Gershunov, A.; Hatchett, B.; Weyant, A.; Dettinger, M.; Su, L.; Rhoades, A.; Williams, P.; Anderson, M.; Rittelmeyer, P.; Lettenmaier, D.; et al. Atmospheric Rivers and Floods in California's Changing Hydroclimate. *San Franc. Estuary Watershed Sci.* **2025**, *23*, 3. [CrossRef]
7. Berg, N.; Hall, A. Increased Interannual Precipitation Extremes over California under Climate Change. *J. Clim.* **2015**, *28*, 6324–6334. [CrossRef]
8. Graves, S.; Bass, B.; Hall, A.; Rahimi, S.; Huang, L. Warming drives streamflow reductions and intensifies hydrologic whiplash, threatening California's water supply. *Earth's Future* **2026**, *14*, e2025EF006985. [CrossRef]
9. California's Climate Change Assessment. Available online: https://www.climateassessment.ca.gov/ (accessed on 1 May 2026).
10. Dettinger, M.; Cayan, D.R. Drought and the California Delta—A Matter of Extremes. *San Franc. Estuary Watershed Sci.* **2014**, *12*, 1–6. [CrossRef]
11. Dettinger, M. Historical and Future Relations Between Large Storms and Droughts in California. *San Franc. Estuary Watershed Sci.* **2016**, *14*, 1. [CrossRef]
12. Pierce, D.W.; Cayan, D.R.; Feldman, D.R.; Risser, M.D. Future increases in North American extreme precipitation in CMIP6 downscaled with LOCA. *J. Hydrometeorol.* **2023**, *24*, 951–975. [CrossRef]
13. Huang, X.; Swain, D.L. Climate change is increasing the risk of a California megaflood. *Sci. Adv.* **2022**, *8*, eabq0995. [CrossRef] [PubMed]
14. Warner, M.D.; Mass, C.F.; Salathe, E.P., Jr. Changes in winter atmospheric rivers along the North American west coast in CMIP5 climate models. *J. Hydrometeor.* **2015**, *16*, 118–128. [CrossRef]
15. Gao, Y.; Lu, J.; Leung, L.R.; Yang, Q.; Hagos, S.; Qian, Y. Dynamical and thermodynamical modulations on future changes of landfalling atmospheric rivers over western North America. *Geophys. Res. Lett.* **2015**, *42*, 7179–7186. [CrossRef]
16. Hamlet, A.F.; Lettenmaier, D.P. Effects of 20th century warming and climate variability on flood risk in the western U.S. *Water Resour. Res.* **2007**, *43*, W06427. [CrossRef]
17. Das, T.; Maurer, E.P.; Pierce, D.W.; Dettinger, M.D.; Cayan, D.R. Increases in flood magnitudes in California under warming climates. *J. Hydrol.* **2013**, *501*, 101–110. [CrossRef]
18. Knowles, N.; Cronkite-Ratcliff, C.; Pierce, D.W.; Cayan, D.R. Responses of unimpaired flows, storage, and managed flows to scenarios of climate change in the San Francisco Bay-Delta watershed. *Water Resour. Res.* **2018**, *54*, 7631–7650. [CrossRef]
19. Bass, B.; Su, L.; Pierce, D.; Rahimi, S.; Hall, A.; Cayan, D.; Krantz, W.; Kalansky, J.; Rhoades, A.; Ullrich, P. Unprecedented Shifts in Hydrology Are Emerging Across California's Critical Basins: An Evaluation from 0.5 to 3.5 °C. *Water Resour. Res.* **2026**, *62*, e2025WR041338. [CrossRef]
20. Cloern, J.E.; Knowles, N.; Brown, L.R.; Cayan, D.; Dettinger, M.D.; Morgan, T.L.; Schoellhamer, D.H.; Stacey, M.T.; van der Wegen, M.; Wagner, R.W.; et al. Projected Evolution of California's San Francisco Bay-Delta-River System in a Century of Climate Change. *PLoS ONE* **2011**, *6*, e24465. [CrossRef] [PubMed]
21. Delta Stewardship Council. *Delta Adapts: Creating a Climate Resilient Future*; Sacramento-San Joaquin Delta Climate Change Vulnerability Assessment; Delta Stewardship Council: Sacramento, CA, USA, 2021.
22. Dettinger, M.; Anderson, J.; Anderson, M.; Brown, L.; Cayan, D.; Maurer, E. Climate change and the Delta. *San Franc. Estuary Watershed Sci.* **2016**, *14*, 4. [CrossRef]

23. Knowles, N.; Cayan, D.R. Potential effects of global warming on the Sacramento/San Joaquin watershed and the San Francisco estuary. *Geophys. Res. Lett.* **2002**, *29*, 38. [CrossRef]
24. Dettinger, M.; Redmond, K.; Cayan, D. Winter Orographic Precipitation Ratios in the Sierra Nevada—Large-Scale Atmospheric Circulations and Hydrologic Consequences. *J. Hydrometeor.* **2004**, *5*, 1102–1116. [CrossRef]
25. Roos, M. A trend of decreasing snowmelt runoff in northern California. In Proceedings of the 59th Western Snow Conference, Juneau, Alaska, 12–16 April 1991; pp. 29–36.
26. Cayan, D.R.; Kammerdiener, S.A.; Dettinger, M.D.; Caprio, J.M.; Peterson, D.H. Changes in the Onset of Spring in the Western United States. *Bull. Amer. Meteor. Soc.* **2001**, *82*, 399–416. [CrossRef]
27. Mote, P.; Hamlet, A.; Clark, M.; Lettenmaier, D. Declining mountain snowpack in Western north America. *Bull. Am. Meteorol. Soc.* **2005**, *86*, 39–49. [CrossRef]
28. Stewart, I.T.; Cayan, D.R.; Dettinger, M.D. Changes toward earlier streamflow timing across western North America. *J. Clim.* **2005**, *18*, 1136–1155. [CrossRef]
29. Kapnick, S.; Hall, A. Causes of recent changes in western North American snowpack. *Clim. Dyn.* **2012**, *38*, 1885–1899. [CrossRef]
30. Mote, P.W.; Li, S.; Lettenmaier, D.P.; Xiao, M.; Engel, R. Dramatic declines in snowpack in the western US. *npj Clim. Atmos. Sci.* **2018**, *1*, 2. [CrossRef]
31. Musselman, K.N.; Addor, N.; Vano, J.A.; Molotch, N.P. Winter melt trends portend widespread declines in snow water resources. *Nat. Clim. Change* **2021**, *11*, 418–424. [CrossRef] [PubMed] [PubMed Central]
32. Shulgina, T.; Gershunov, A.; Hatchett, B.J.; Guirguis, K.; Subramanian, A.C.; Margulis, S.A.; Fang, Y.; Cayan, D.R.; Pierce, D.W.; Dettinger, M.; et al. Observed and projected changes in snow accumulation and snowline in California's snowy mountains. *Clim. Dyn.* **2023**, *61*, 4809–4824. [CrossRef]
33. Knowles, N.; Cayan, D.R. Elevational dependence of projected hydrologic changes in the San Francisco estuary and watershed. *Clim. Change* **2004**, *62*, 319–336. [CrossRef]
34. Pierce, D.W.; Cayan, D.R. The Uneven Response of Different Snow Measures to Human-Induced Climate Warming. *J. Clim.* **2013**, *26*, 4148–4167. [CrossRef]
35. Rhoades, A.M.; Jones, A.D.; Ullrich, P.A. The changing character of the California Sierra Nevada as a natural reservoir. *Clim. Change* **2018**, *148*, 387–422.
36. Sun, F.; Berg, N.; Hall, A.; Schwartz, M.; Walton, D. Understanding end-of-century snowpack changes over California's Sierra Nevada. *Geophys. Res. Lett.* **2019**, *46*, 933–943. [CrossRef]
37. Cho, E.; McCrary, R.R.; Jacobs, J.M. Future changes in snowpack, snowmelt, and runoff potential extremes over North America. *Geophys. Res. Lett.* **2021**, *48*, e2021GL094985. [CrossRef]
38. Siirila-Woodburn, E.R.; Rhoades, A.M.; Hatchett, B.J.; Huning, L.S.; Szinai, J.; Tague, C.; Nico, P.S.; Feldman, D.R.; Jones, A.D.; Collins, W.D.; et al. A low-to-no snow future and its impacts on water resources in the western United States. *Nat. Rev. Earth Environ.* **2021**, *2*, 800–819. [CrossRef]
39. Rhoades, A.M.; Hatchett, B.J.; Risser, M.D.; Collins, W.D.; Bambach, N.E.; Huning, L.S.; McCrary, R.; Siirila-Woodburn, E.R.; Ullrich, P.A.; Wehner, M.F.; et al. Asymmetric emergence of low-to-no snow in the midlatitudes of the American Cordillera. *Nat. Clim. Change* **2022**, *12*, 1151–1159. [CrossRef]
40. Livneh, B.; Rosenberg, E.A.; Lin, C.; Nijssen, B.; Mishra, V.; Andreadis, K.M.; Maurer, E.P.; Lettenmaier, D.P. A long-term hydrologically based dataset of land surface fluxes and states for the conterminous United States: Update and extensions. *J. Clim.* **2013**, *26*, 9384–9392. [CrossRef]
41. Liang, X.; Lettenmaier, D.P.; Wood, E.F.; Burges, S.J. A simple hydrologically based model of land surface water and energy fluxes for general circulation models. *J. Geophys. Res.* **1994**, *99*, 14415–14428. [CrossRef]
42. Schaperow, J.R.; Li, D.; Margulis, S.A.; Lettenmaier, D.P. A near-global, high resolution land surface parameter dataset for the variable infiltration capacity model. *Sci. Data* **2021**, *8*, 216. [CrossRef] [PubMed]
43. California Office of Planning and Land Use. Available online: https://lci.ca.gov/climate/icarp/climate-assessment/ (accessed on 1 January 2024).
44. Bass, B.; Su, L.; Lettenmaier, D. *Data Adoption Justification Memo (for California's Fifth Climate Change Assessment): Hydrology Projections*; California Energy Commission: Sacramento, CA, USA, 2023. Available online: https://www.energy.ca.gov/sites/default/files/2025-04/05_HydrologyProjections_DataJustificationMemo_BassEtAl_Adopted_v3_ada.pdf (accessed on 26 April 2024).
45. Su, L.; Lettenmaier, D.P.; Pan, M.; Bass, B. Improving runoff simulation in the Western United States with Noah-MP and variable infiltration capacity. *Hydrol. Earth Syst. Sci.* **2024**, *28*, 3079–3097.
46. Tolson, B.A.; Shoemaker, C.A. Dynamically dimensioned search algorithm for computationally efficient watershed model calibration. *Water Resour. Res.* **2007**, *43*, W01413. [CrossRef]

47. Pierce, D.W.; Rahimi, S.; Iacobellis, S.; Cayan, D.R.; Kalansky, J. LOCA Version 2 Training Data. Data Adoption Justification Memo (for California's Fifth Climate Change Assessment. 2023. Available online: https://www.energy.ca.gov/sites/default/files/2024-03/03_LOCA2-forCA-TrainingData_DataJustificationMemo_Pierce_Adopted_ada.pdf (accessed on 30 April 2023).
48. Kling, H.; Fuchs, M.; Paulin, M. Runoff conditions in the upper Danube basin under an ensemble of climate change scenarios. *J. Hydrol.* **2012**, *424*, 264–277. [CrossRef]
49. California Department of Water Resources (DWR). California Data Exchange Center: Daily Full Natural Flow [Dataset]. 2023. Available online: https://cdec.water.ca.gov/reportapp/javareports?name=FNF (accessed on 15 July 2026).
50. Bohn, T.J.; Livneh, B.; Oyler, J.W.; Running, S.W.; Nijssen, B.; Lettenmaier, D.P. Global evaluation of MTCLIM and related algorithms for forcing of ecological and hydrological models. *Agric. For. Meteorol.* **2013**, *176*, 38–49. [CrossRef]
51. Thornton, P.E.; Running, S.W. An improved algorithm for estimating incident daily solar radiation from measurements of temperature; humidity, and precipitation. *Agric. For. Meteorol.* **1999**, *93*, 211–228. [CrossRef]
52. Krantz, W.; Pierce, D.; Goldenson, N.; Cayan, D. Memorandum on evaluating global climate models for studying regional climate change in California. *Tech. Rep.* **2021**, *6*, 1–24.
53. Lehner, F.; Deser, C.; Maher, N.; Marotzke, J.; Fischer, E.M.; Brunner, L.; Knutti, R.; Hawkins, E. Partitioning climate projection uncertainty with multiple large ensembles and CMIP5/6. *Earth Syst. Dyn.* **2020**, *11*, 491–508. [CrossRef]
54. Kalansky, J.F.; Yao, P.; Pierce, D.W.; Cayan, D.R. Memo on General Use Projections. Deliverable to the California Energy Commission. 2024. Available online: https://www.energy.ca.gov/media/10478 (accessed on 24 September 2024).
55. Pierce, D.W.; Cayan, D.R.; Maurer, E.P.; Abatzoglou, J.T.; Hegewisch, K.C. Improved Bias Correction Techniques for Hydrological Simulations of Climate Change. *J. Hydromet.* **2015**, *16*, 2421–2442. [CrossRef]
56. Pierce, D.W.; Rahimi, S.; Cayan, D.R.; Kalansky, J. Bias Correction in the WRF and LOCA Version 2 Projections. Data Adoption Justification Memo (for California's Fifth Climate Change Assessment). 2024. Available online: https://www.energy.ca.gov/sites/default/files/2024-03/01_BiasCorrectioninWRF_and_LOCA2Projections_DataJustificationMemo_Pierce_Adopted_ada.pdf (accessed on 26 April 2024).
57. Pierce, D.W.; Cayan, D.R.; Thrasher, B.L. Statistical downscaling using Localized Constructed Analogs (LOCA). *J. Hydrometeorol.* **2014**, *15*, 2558–2585. [CrossRef]
58. Pierce, D.W.; Cayan, D.R.; Rahimi, S.; Kalansky, J. LOCA Version 2 Hybrid Downscaling. Data Adoption Justification Memo (for California's Fifth Climate Change Assessment). 2024. Available online: https://www.energy.ca.gov/sites/default/files/2024-06/02_DynamicalDownscaling_DataJustificationMemo_Rahimi_Adopted_v2May2024_ada.pdf (accessed on 26 April 2024).
59. Williams, A.P.; McKinnon, K.A.; Anchukaitis, K.J.; Gershunov, A.; Varuolo-Clarke, A.M.; Clemesha, R.E.S.; Liu, H. Anthropogenic intensification of cool-season precipitation is not yet detectable across the Western United States. *J. Geophys.* **2024**, *129*, e2023JD040537. [CrossRef]
60. Held, I.M.; Soden, B.J. Robust responses of the hydrological cycle to global warming. *J. Clim.* **2006**, *19*, 5686–5699. [CrossRef]
61. Prein, A.F.; Rasmussen, R.M.; Ikeda, K.; Liu, C.; Clark, M.P.; Holland, G.J. The future intensification of hourly precipitation extremes. *Nat. Clim. Change* **2017**, *7*, 48–52. [CrossRef]
62. Dettinger, M.D.; Ralph, F.M.; Das, T.; Neiman, P.J.; Cayan, D.R. Atmospheric rivers, floods and the water resources of California. *Water* **2011**, *3*, 445–478. [CrossRef]
63. Dettinger, M.D.; Rajagopal, S. Simulated Hydrologic Responses to Climate-Change Projections for the Lake Tahoe Basin: Subbasin-Scale Results. Desert Research Institute Publication 41292, Prepared for California Tahoe Conservancy. 2023. Available online: https://www.mdettinger.com/_files/ugd/3b5c57_39f4f3da5cf241788baa09ac85cd4490.pdf (accessed on 16 August 2026).
64. Shukla, S.; Steinemann, A.; Iacobellis, S.F.; Cayan, D.R. Annual Drought in California: Association with Monthly Precipitation and Climate Phases. *J. Appl. Meteor. Climatol.* **2015**, *54*, 2273–2281. [CrossRef]
65. Ralph, F.M.; James, J.; Leahigh, J.; Anderson, M.; Talbot, C.; Haynes, A.; Forbis, J.; White, M.; Lindley, S. *Yuba-Feather Forecast Informed Reservoir Operations: Preliminary Viability Assessment*; University of California San Diego: La Jolla, CA, USA, 2022; Volume 129. Available online: https://escholarship.org/uc/item/8x57n58b (accessed on 17 August 2026).
66. California Department of Water Resources. San Joaquin Basin FloodMAR Studies, Merced Watershed Study Area Report. 2025. Available online: https://cadwr.app.box.com/s/1mmbblsok46ljheicf0kmfx7q3hhhng2/file/2056816530315?sb=/details (accessed on 17 August 2026).
67. Brewer, W.H.; Farquhar, F.P. *Up and Down California in -1864*; Yale University Press: New Haven, CT, USA; Oxford University Press: London, UK, 1930. Available online: https://www.loc.gov/item/30029264/ (accessed on 15 June 2026).
68. Roos, M. *The Great New Year's Flood of 1997 in Northern California*; California Extreme Precipitation Symposium: Rocklin, CA, USA, 1997; Available online: https://cepsym.org/Sympro1997/Roos.pdf (accessed on 15 June 2026).
69. Kelley, R.L. *Battling the Inland Sea Floods, Public Policy, and the Sacramento Valley*; University of California Press: Berkeley, CA, USA, 1997; 426p.

70. Fish, M.A.; Wilson, A.M.; Ralph, F.M. Atmospheric River Families: Definition and Associated Synoptic Conditions. *J. Hydrometeor.* **2019**, *20*, 2091–2108. [CrossRef]
71. Brandt, W.T.; Haleakala, K.; Hatchett, B.J.; Pan, M. A Review of the Hydrologic Response Mechanisms During Mountain Rain-on-Snow. *Front. Earth Sci.* **2022**, *10*, 791760. [CrossRef]

Disclaimer/Publisher's Note: The statements, opinions and data contained in all publications are solely those of the individual author(s) and contributor(s) and not of MDPI and/or the editor(s). MDPI and/or the editor(s) disclaim responsibility for any injury to people or property resulting from any ideas, methods, instructions or products referred to in the content.